

# Chemical Science

Accepted Manuscript

This article can be cited before page numbers have been issued, to do this please use: S. K. Dave and S. Stecko, *Chem. Sci.*, 2026, DOI: 10.1039/D5SC08559D.



This is an Accepted Manuscript, which has been through the Royal Society of Chemistry peer review process and has been accepted for publication.

Accepted Manuscripts are published online shortly after acceptance, before technical editing, formatting and proof reading. Using this free service, authors can make their results available to the community, in citable form, before we publish the edited article. We will replace this Accepted Manuscript with the edited and formatted Advance Article as soon as it is available.

You can find more information about Accepted Manuscripts in the [Information for Authors](#).

Please note that technical editing may introduce minor changes to the text and/or graphics, which may alter content. The journal's standard [Terms & Conditions](#) and the [Ethical guidelines](#) still apply. In no event shall the Royal Society of Chemistry be held responsible for any errors or omissions in this Accepted Manuscript or any consequences arising from the use of any information it contains.

# Remote $\alpha$ - and $\beta$ -C(sp<sup>3</sup>)-H Alkenylation of Amines via Visible-Light Supported Paired Electrolysis

View Article Online  
DOI: 10.1039/D5SC08559D

Siddharth K. Dave, and Sebastian Stecko\*

Institute of Organic Chemistry, Polish Academy of Sciences

Marcina Kasprzaka Street 44/52, 01-224 Warsaw, Poland

E-mail: [sebastian.stecko@icho.edu.pl](mailto:sebastian.stecko@icho.edu.pl)

## Abstract

A general method for photoelectrochemical site-selective  $\alpha$ - and  $\beta$ -C(sp<sup>3</sup>)-H alkenylation of amines with vinyl bromides has been developed. Regioselective activation of inert C-H bonds is achieved by intramolecular hydrogen atom abstraction (HAT) by an oxidatively generated aryl radical. Depending on the HAT directing group attached to the amines' N-atom, either 1,5- or 1,6-H-atom transposition occurred, leading to regiosomeric carbon-centered radical species. C-radicals thus formed at the  $\alpha/\beta$ -position of the amines' functionality undergo radical cross-coupling with Ni complex-activated vinyl bromide to provide the corresponding  $\alpha$ - or  $\beta$ -functionalized amines. Good functional group tolerance, the gram-scale experiments, post-functionalization and demonstration of preparation of key structural scaffolds of the selected naturally occurring compounds and drug candidates greatly highlight the potential applicability of the presented method. The mechanistic experiments demonstrated that the reported protocol consists of a photoelectrochemically induced thiyl radical anodic cycle and an electrochemically driven Ni-catalytic cathodic cycle. The first one is responsible for the generation of CO<sub>2</sub><sup>•-</sup>, a XAT reagent capable of activation of aryl halide to provide aryl radical species. Cathodic reduction of a Ni(I) intermediate to the Ni(0) complex allows closing the Ni-catalyzed cycle, enabling the execution of the cross-coupling stage leading to a C-H functionalized amine derivative. The developed conditions enable precise synchronization of anodic and cathodic catalytic cycles occurring in the presented variant of paired electrolysis, which has been a significant challenge until now.

**Keywords:** photoelectrolysis, pair electrolysis, hydrogen atom transfer, amines, vinyl halides, C-H functionalization, radical reactions, Ni-catalysis.

## Introduction

The allylic amine moiety is a ubiquitous structural motif found in numerous bioactive molecules and naturally occurring compounds like anticancer maclekarpine E,<sup>1, 2</sup> antimicrobial zanthocapsine<sup>2, 3</sup>,<sup>4</sup> or alkaloid caulophyllumine<sup>5</sup> (Figure 1). Furthermore, allylamines are versatile intermediates and building blocks, with numerous applications in organic synthesis. For instance, alkenylated heterocyclic scaffolds often serve as a direct precursor for a total synthesis of numerous alkaloids (e.g., galipeine,<sup>6</sup>,<sup>7</sup> cuspareine,<sup>6</sup> galipininine,<sup>6</sup> angustureine,<sup>6</sup> dysoxyline,<sup>8, 9</sup> methofoline<sup>8, 9</sup>) or heterocyclic drugs (e.g., almorexant,<sup>10, 11</sup> inferanserin,<sup>12</sup> encainide<sup>13, 14</sup>) presented in Figure 1.

Classic methods for allylamine synthesis rely on nucleophilic substitution by amines<sup>15, 16</sup> including Tsuji-Trost allylic amination,<sup>15, 17-19</sup> vinylation of imines,<sup>20, 21</sup> reductive amination of enals or enones,<sup>22</sup> or sigmatropic rearrangement reactions.<sup>23,24, 25</sup> Although these are well-established protocols in synthetic organic chemistry, they also exhibit several drawbacks, like the use of stoichiometric amounts of organometallic reagents, insufficient levels of stereocontrol, or the formation of numerous side products. So far, the Pd- or Ir-catalyzed Tsuji-Trost allylic amination reaction seems to be the most efficient strategy to deliver linear or branched allylamines (depending on the metal catalyst used) by reacting amines with various allylic electrophiles.<sup>15, 17-19</sup> Nevertheless, even this strategy still encounters challenges and drawbacks, particularly in the preparation of  $\alpha$ -alkenylated saturated aza-heterocycles.

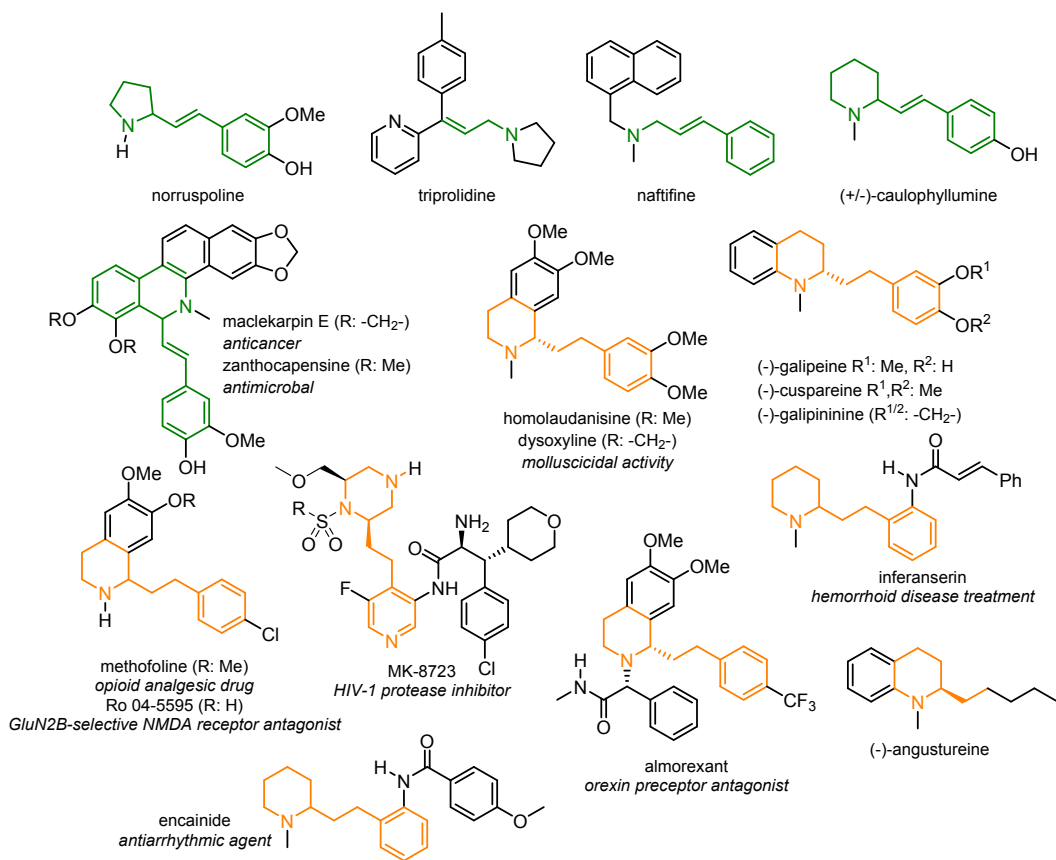
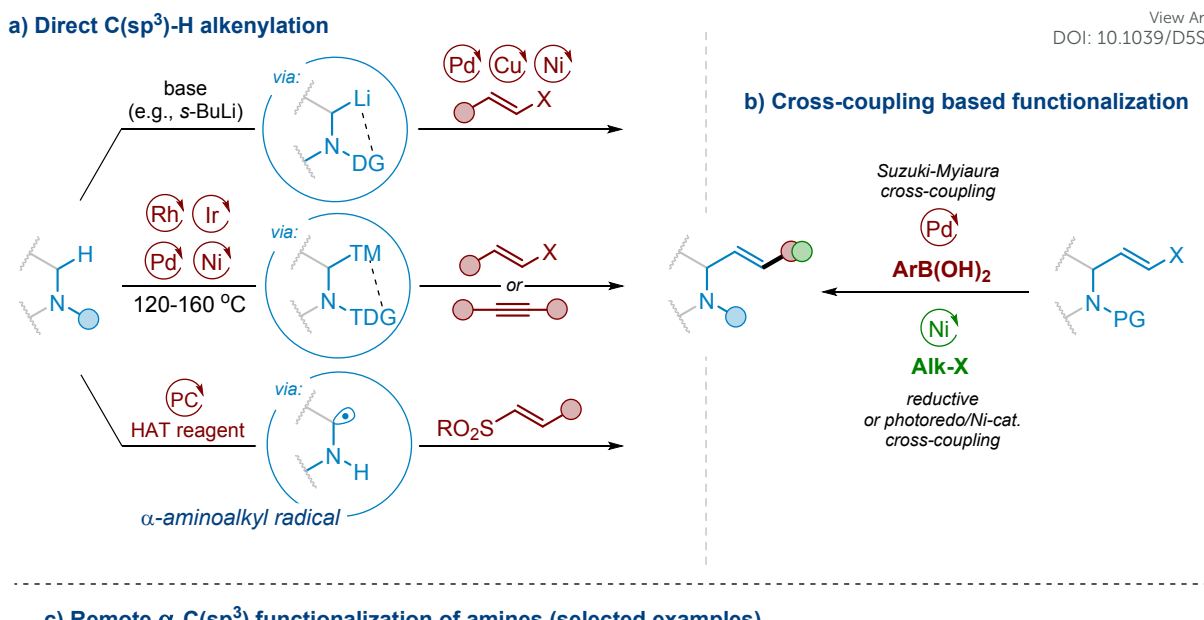


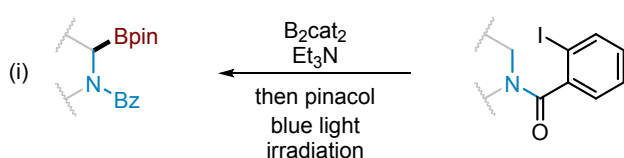
**Figure 1.** Representative bioactive compounds containing allylic amine moiety (in green) and bioactive molecules obtained from the corresponding allylamine precursors (in yellow).



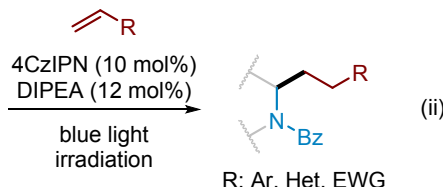


**c) Remote  $\alpha$ -C(sp<sup>3</sup>) functionalization of amines (selected examples)**

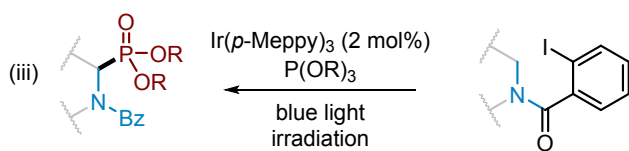
$\alpha$ -C-H borylation (Gevorgyan *et al.*, 2022)



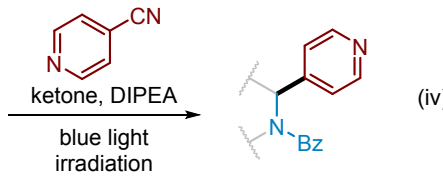
Giese-type  $\alpha$ -C-H alkylation (Saget *et al.*, 2023)



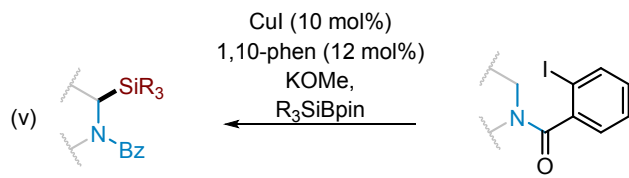
Arbuzov-type  $\alpha$ -C-H phosphorylation (Zhang & Wu *et al.*, 2023)



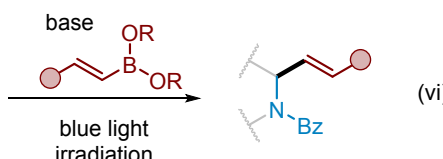
$\alpha$ -C-H hetero-arylation (Yatham *et al.*, 2024)



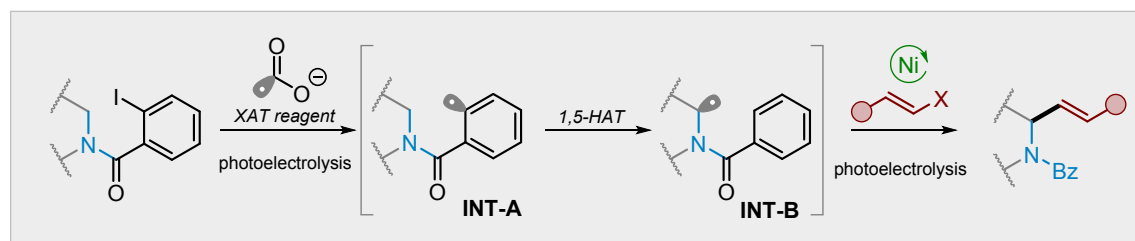
$\alpha$ -C-H silylation (Zhang & Guo *et al.*, 2024)



$\alpha$ -C-H alkenylation (Zhang & Guo *et al.*, 2024)



This work: Photoelectrochemical C(sp<sup>3</sup>)-H alkenylation of amines



**Scheme 1.** Background and concept design: a) Traditional direct  $\alpha$ -C(sp<sup>3</sup>)-H alkenylation of amines; b) Divergent functionalization of allylamine vinyl bromides; c) remote  $\alpha$ -C(sp<sup>3</sup>)-H functionalization of amines.

From the synthetic perspective, direct regio- and stereoselective  $\alpha$ -C(sp<sup>3</sup>)-H alkenylation is regarded as the most attractive strategy for synthesizing the mentioned types of allylamines since it starts with inexpensive, readily available cyclic amines (Scheme 1a).<sup>26, 27, 28</sup> The classic approaches involve deprotonation by organolithium reagents, followed by transition metal-mediated cross-coupling with vinyl halide reagents (Scheme 1a). An alternative approach is direct C-H bond activation by transition metal complexes followed by coupling with a vinyl reagent (Scheme 1a).<sup>28</sup> Alkynes, in addition to vinyl halides, can serve as effective alkenylating agents (Scheme 1a).<sup>28, 29, 30</sup> Nevertheless, the use of a strong base significantly limits the substrate scope in the first case, whereas the requirement of expensive metal complexes and harsh reaction conditions significantly limits the efficiency of the second process. Moreover, both cases require specific directing groups to achieve regioselective activation of the  $\alpha$ -C-H bond, and these groups must be removed in further steps. A less explored approach for the synthesis of complex allylamines relies on a functionalization, for instance arylation or alkylation, of allylamine derivatives, e.g., allylamine vinyl bromides, through their reactions with arylating agents (e.g., arylboronic acids)<sup>31-33</sup> or alkylating reagents<sup>18a, 33</sup>, including alkyl radical precursors (e.g., alkyl halides, carboxylic acids etc.) under photoredox<sup>34, 35</sup> (Scheme 1b).

Intensive developments in modern organic photochemistry brought new concepts in the synthesis of allylamines, particularly methods involving the generation and alkenylation of  $\alpha$ -aminoalkyl radical species (Scheme 1a). In their pioneering works, MacMillan and co-workers<sup>36, 37</sup> demonstrated conditions for Ir-catalysed photoredox vinylation of tertiary *N*-aryl amines with vinyl sulfones. The key intermediates,  $\alpha$ -aminoalkyl radical species, were generated either from amines via an SET/deprotonation sequence or through the decarboxylation of amino acids, mediated by a photoexcited Ir complex acting as a strong oxidant. A few years later, Xie and co-workers<sup>38</sup> employed this approach for the total synthesis of maclekarpine E (Fig. 1) and its analogues.

The intramolecular 1,5-hydrogen atom transfer (1,5-HAT) strategy is another method for the generation of  $\alpha$ -aminoalkyl radical species (e.g., **INT-B**).<sup>39-45</sup> It has recently gained a lot of attention as a powerful tool for selective C-H bond functionalisation, introducing various functional groups, and delivering complex molecules. This method often involves using a substrate with a pre-installed functional group that operates as a source of reactive radical intermediates (e.g., **INT-A**), serves as a directing group to control the 1,5-HAT process, and acts as a protective group. In 2022, Gevorgyan and his team<sup>46</sup> reported a simple and effective method for adding a boron group to the  $\alpha$ -C-H bond of 2-iodobenzoyl-protected secondary amines, resulting in the formation of  $\alpha$ -amino boronic acids (Scheme 1c, (i)). The key step of this process was single-electron transfer (SET) or halogen-atom transfer (XAT) cleavage of C(sp<sup>2</sup>)-I bond to generate an aryl radical (e.g., **INT-A**). This species is capable of subsequent 1,5-hydrogen atom abstraction from the  $\alpha$ -C position of secondary amine. The trapping agent, such as B<sub>2</sub>cat<sub>2</sub>, then intercepts the resulting alkyl radical (e.g., **INT-B**) to produce a functionalised product. Soon after, Zhang's group<sup>47</sup> demonstrated a visible-light-induced asymmetric C(sp<sup>3</sup>)-H Cu-catalysed



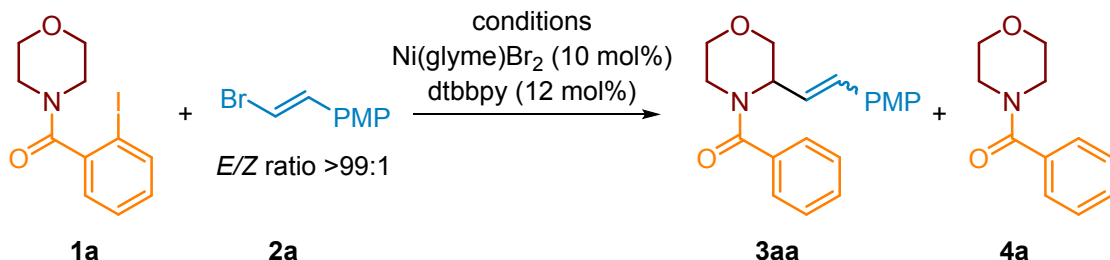
alkynylation of cyclic tertiary amines initiated by the 1,5-HAT process. After this research, both the Wang group<sup>48</sup> and the Saget group (Scheme 1c, (ii))<sup>49</sup> and others developed similar methods, using aryl radicals to start the 1,5-HAT process for the  $\alpha$ -C-H functionalisation of secondary amines with Michael acceptors, while Sureshkumar and others reported the conditions for photoredox  $\alpha$ -C-H alkylation using [1.1.1]-propellane.<sup>50</sup> Several reports also describe the  $\alpha$ -C-H arylation method through cross-coupling of  $\alpha$ -aminoalkyl radicals with heteroarenes. The pool of potent trapping agents that can be used for such radical remote C-H functionalisation includes phosphites ( $\alpha$ -C-H phosphonation, Scheme 1c, (iii)),<sup>51</sup> aldehydes ( $\alpha$ -C-H acylation),<sup>52</sup> silyl reagents ( $\alpha$ -C-H silylation, Scheme 1c, (v)),<sup>53</sup> imines ( $\alpha$ -C-H aminoalkylation) and azides ( $\alpha$ -C-H azidation).<sup>54</sup> Surprisingly, the analogous concept for  $\alpha$ -C-H alkenylation of cyclic amines is almost unknown so far, with only one report on the related aryl radical-mediated  $\alpha$ -C(sp<sup>3</sup>)-H alkenylation of secondary amines by Guo, Zhang, and their co-workers (Scheme 1c, (vi)).<sup>55</sup> They employed the ate complexes of vinylboronic acid esters and alkoxides as alkenylation agents. This ate complex interacted with the secondary amine substrate to deliver the EDA complex, which underwent photoexcitation to generate an aryl radical from the 2-iodobenzoyl group attached to the amine nitrogen atom. The subsequent 1,5-HAT process produced the desired 2-alkenylated products in excellent yield by intercepting the alkyl radical with the activated alkenylboronic acid. Although this method is quite elegant, some drawbacks related to the employed reaction conditions still leave a space for further improvements and advancements in terms of substrate diversity, cost-effectiveness, and reaction selectivity.

We questioned if vinyl halides, instead of vinyl boronic acid derivatives, could serve as suitable reagents for the aforementioned C-H alkenylation of secondary amines through the 1,5-HAT/cross-coupling sequence facilitated by aryl radicals. Based on the previous reports, we decided to use the 2-halogenbenzoyl group to produce aryl radicals, which should deliver the  $\alpha$ -aminoalkyl radical after the 1,5-HAT process; this radical is designed to react with the Ni(II)-alkene complex generated from the vinyl halide and Ni(0). Our primary objective was to establish conditions suitable for the activation of both reaction partners. This phase appeared to be the most challenging, as the Ni(0) complex may activate both the vinyl halide and the aryl halogen moiety of the HAT-directing group. Consequently, our primary task was to develop conditions for the effective activation of the directing group and the ensuing cross-coupling process with activated vinyl halide. The next objective was to synchronise all three steps: aryl radical generation, 1,5-HAT and cross-coupling within the specified sequence. This issue was critical because failing to meet the correct conditions may predominantly lead to undesired homocoupling and dehalogenation products from the starting materials, resulting in a complex reaction mixture.

## Results and Discussion

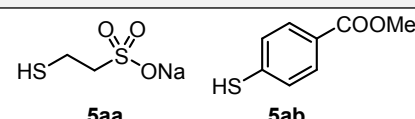
**Reaction conditions development.** With our hypothesis in mind, we started exploring the feasibility of our proposed alkenylation reaction. We chose 2-iodobenzoyl-protected morpholine **1a** and vinyl bromide **2a** as model substrates. The reaction between them was performed in the presence of Ni(glyme)Br<sub>2</sub> (10 mol%) and 4,4'-di-*t*-butyl-2,2'-bipyridine (dtbbpy) (12 mol %) which formed the corresponding Ni-complex for the final cross-coupling step.<sup>34, 56</sup>





Ent.	Conditions	Conv. of 1a	Yield of 3aa	Yield of 4a	Ref.
1a.	[Ir(ppy) <sub>2</sub> (dtbbpy)]PF <sub>6</sub> (1 mol%), K <sub>3</sub> PO <sub>4</sub> (3 eq), MeCN, 26 °C, TBABr (5 eq), blue light irradiation (450–460 nm)	>99%	traces (GC)	87% (isol.)	<sup>57, 58</sup>
1b.	[Ir(dF(CF <sub>3</sub> )ppy) <sub>2</sub> (dtbbpy)]PF <sub>6</sub> (1 mol%), Hantzsch's ester (3 eq), MeCN, 26 °C, blue light irradiation (450–460 nm)	>99%	traces (GC)	90% (isol.)	<sup>59</sup>
2a.	4-CzIPN (2 mol%), <i>i</i> -Pr <sub>2</sub> NEt (3 eq), DMSO, 26 °C, blue light irradiation (450–460 nm)	45%	traces (GC)	27% (isol.)	<sup>60</sup>
2b.	4-CzIPN (2 mol%), Et <sub>3</sub> N (3 eq), DMSO, 26 °C, blue light irradiation (450–460 nm)	57%	traces (GC)	33% (isol.)	-
2c.	4-CzIPN (2 mol%), <i>n</i> -Bu <sub>3</sub> N (3 eq), DMSO, 26 °C, blue light irradiation (425 nm)	61%	traces (GC)	41% (isol.)	-
3a.	TTMS (2 eq), DCE, 26 °C, blue light irradiation (450–460 nm)	>99%	traces (GC)	90% (isol.)	<sup>61</sup>
3b.	4-CzIPN (2 mol%), TTMS (2 eq), DCE, 26 °C, blue light irradiation (450–460 nm)	>99%	traces (GC)	89% (isol.)	-
4a.	Cs <sub>2</sub> CO <sub>3</sub> (3 eq), DMSO, 26 °C, blue light irradiation (440 nm)	0%	0% (GC)	0% (GC)	<sup>50</sup>
4b.	Cs <sub>2</sub> CO <sub>3</sub> (3 eq), DMSO, 26 °C, blue light irradiation (395 nm)	>99%	<10% (GC)	70% (isol.)	-
4c.	Cs <sub>2</sub> CO <sub>3</sub> (3 eq), DMSO, 26 °C, blue light irradiation (365 nm)	>99%	traces (GC)	83% (isol.)	-
5	4-DPAIPN (2 mol%), mesna <b>5aa</b> (20 mol%), HCOOCs (3 eq), DMSO, blue light irradiation (440 nm)	>99%	~15% (NMR)	68% (isol.)	<sup>62</sup>
6a.	(+)Ni Graphite(-), TBACl (1 eq), DMF, rt, 15 mA, 6 h	>99%	traces (GC) <sup>b</sup>	35% (isol.)	<sup>63</sup>
6b.	(+)Zn Graphite(-), TBABF <sub>4</sub> (1 eq), DMSO/MeCN 9:1 v/v, 40 °C, 9 mA, 4 h	90%	traces (GC) <sup>b</sup>	62% (isol.)	<sup>64</sup>
6c.	(+)Graphite SS(-), TBABF <sub>4</sub> (1 eq), phenanthrene (1 eq), MeCN 12 mA, 4 h	92%	traces (GC) <sup>b</sup>	55% (isol.)	<sup>65</sup>
6d.	(+)RVC Ni <sub>foam</sub> (-), TBABF <sub>4</sub> (2 eq), HCOOCs (3 eq.), thiol <b>5ab</b> (30 mol%), DMSO, 28 °C, 3 mA, irradiation (395 nm), 12 h	91%	35% (GC) <sup>c</sup>	43% (isol.)	-

<sup>a</sup> determined by GC, <sup>b</sup> formation of homo- and cross-coupling products; <sup>c</sup> the E/Z ratio 81:19; DCE = dichloroethane; TTMS = (TMS)<sub>2</sub>SiH; ppy = 2-phenylpyridine; dtbbpy = 4,4'-di-*t*-butyl-2,2'-bipyridine; SS = stainless steel, PMP = 4-methoxyphenyl.



**Scheme 2.** Screening of initial conditions. PMP = 4-methoxyphenyl.

Initially, we examined diverse photochemical conditions for the reductive generation of aryl radical **INT-A**. In preliminary studies, we adapted the conditions for a generation of aryl radicals described by Doyle<sup>57, 58</sup> and others<sup>59</sup> and the alkenylation of **1a** with **2a** was conducted using an Ir complex, as a photocatalyst, and K<sub>3</sub>PO<sub>4</sub> as a base and TBABr as a source as a Br radical acting as XAT reagent. The model reaction was performed in MeCN under blue light irradiation (450–460 nm) (Scheme 2, ent. 1a). While complete conversion of **1a** took place, only traces of desired product **3aa** were detected (as determined by GC analysis), alongside the deiodination product **4a** and the homocoupling product of vinyl bromide **2a**. Further modifications to these reaction conditions, including variations in the nickel source (e.g., Ni(glyme)Cl<sub>2</sub>, Ni(cod)<sub>2</sub>, NiI<sub>2</sub>, etc.), base (K<sub>2</sub>CO<sub>3</sub>, K<sub>2</sub>HPO<sub>4</sub>, KH<sub>2</sub>PO<sub>4</sub>, Na<sub>2</sub>CO<sub>3</sub>, etc.), or solvent(s) (e.g., DMF, MeCN, etc.), failed to enhance the process, with product **4a** remaining predominant. Next, we turned our attention on the Leonori studies<sup>60</sup> revealing trialkylamines as potent



XAT reagents for the generation of aryl radicals from the corresponding aryl halides.<sup>49,66</sup> Adapting the Leonori report,<sup>60</sup> the model alkenylation reaction was conducted with 4-CzIPN as a photocatalyst and Hünig's base as an XAT reagent. Unluckily, the conversion of **1a** was quite low (45%) and again merely traces from the expected product was detected (Scheme 2, ent. 2a). Furthermore, any further modifications to the reaction conditions, such as altering the photocatalyst (e.g., 4-DPAIPN,<sup>67, 68</sup> 3-DPA(F)IPN, 4-Cl-CzIPN,  $[\text{Ir}(\text{dFppy})_2(\text{dtbbpy})]\text{PF}_6$ ) or changing the employed trialkylamine reagent (e.g.,  $\text{Et}_3\text{N}$ ,  $n\text{-Bu}_3\text{N}$ , etc.), were unsatisfactory. The same result was obtained when the HAT reagent, aryl radical, was formed via a  $\text{C}(\text{sp}^2)\text{-I}$  bond cleavage by a silyl radical, as reported by Yang and Guo.<sup>69,70</sup> In this case, tris(trimethylsilyl)silane (TTMS) acted as a source of an XAT reagent produced photochemically with or without a photocatalyst (Scheme 2, ent. 3a and 3b). Under both conditions, the competitive reductive dehalogenation of the heterocyclic substrate occurred more rapidly than the expected Ni-catalyzed cross-coupling process. We have also examined the protocol outlined by Sureshkumar,<sup>50</sup> wherein 2-iodobenzoyl-protected amines, e.g. **1a**, form with the carbonate anion an electron donor-acceptor complex (EDA complex), which upon irradiation (440 nm) should undergo photoexcitation and generate the aryl radical (via homolysis of C-I bond) for the subsequent 1,5-HAT step.

Disappointingly, upon implementing the specified conditions (Scheme 2, ent. 4a), we neither observed the generation of product **3aa** nor even product **4a**, and recovered entire starting material **1a**. Our spectroscopic studies confirmed that compound **1a** forms the postulated by authors EDA complex with carbonate ions, as indicated by the bathochromic shift of the absorption band for **1a** from ca. 290 nm to 332 nm (see e-SI, Fig. SI-8). Nonetheless, this maximum is evidently beyond the spectrum of the light source employed by the authors (Kessil™ LED Lamp 440 nm<sup>71</sup>), hence precluding any potential for photoexcitation of the specified complex!

In light of the above observations and evidences, we decided to repeat this experiment using higher-energy light sources. Upon irradiating the reaction mixture with light at a wavelength of 395 nm (Scheme 2, ent. 4b), we observed complete conversion of the substrate **1a**, but the yields of the desired product **3aa** were below 10%. Similarly, when irradiating with light at a wavelength of 365 nm (Scheme 2, ent. 4c), substrate **1a** underwent complete conversion, however only traces of **3a** were noticed by a GC analysis.

Lack of success of a photochemical approach forced us to investigate the generation of aryl radical for 1,5-HAT process under electrochemical conditions either via direct or electromediator-aided pathway (Scheme 2, ent. 6a-6d).<sup>72,73, 74</sup> Following the protocol for an electroreduction of aryl iodides reported by Wang,<sup>63</sup> we electrolyzed the model reaction mixture in electrochemical cell equipped with Ni-anode and graphite cathode (Scheme 2, ent. 6a), however mostly we observed a formation of homo- and cross-coupling product. The further modification of reaction conditions, like change of electrolyte, solvent did not provide significant improvement. The change of a sacrificial anode material into Zn,<sup>64</sup> Al,<sup>75</sup> Mg<sup>76</sup> or steel<sup>65</sup> along with an use of electromediator, e.g., phenanthrene, provided 10-15% of the desired product along with homo-/cross-coupling side products. An important observation from these experiments was a high conversion of **1a**, although, a formation of **3aa** and deiodination product **4a** was

Open Access Article. Published on 21 January 2026. Downloaded on 1/25/2026 3:10:21 AM.  
This article is licensed under a Creative Commons Attribution-NonCommercial 3.0 Unported Licence.

not noticed. Instead of that we observe the formation of a mixture of homo- and cross-coupling products of **1a** and **2a** indicating that examined electrochemical conditions are capable to execute efficiently Ni-catalytic cycle, plausibly due to reduction of Ni(I) species to key Ni(0) one.

Finally, we turned our attention on a reduction of aryl halides by carbon dioxide radical anion ( $\text{CO}_2^{\cdot-}$ ). This radical species is valuable synthetic intermediate; thanks to extremely negative reduction potential ( $E_{1/2(\text{red})}(\text{CO}_2/\text{CO}_2^{\cdot-}) = -2.2$  V vs. SCE)<sup>77</sup> and reactivity that makes it an efficient reductant and carboxylating agent.<sup>78</sup> Moreover, it can be easily generated from readily available formats by photoredox-HAT protocols in the presence of photocatalysts and additional hydrogen transfer reagents, commonly thiols.<sup>78</sup>

Initially, we employed the protocol for a photoinduced remote Giese-type C-H alkylation of amines in the presence of HCOOCs, reported by Yatham *et al.*<sup>79</sup> Thus, the mixture of model substrates **1a** and **2a** along with Ni-complex and HCOOCs in DMSO was irradiated with purple light (390 nm). The starting material **1a** was consumed completely after 12 h to provide mostly product **4a** along with traces of **3aa** and small amounts of cross- or homo-coupling products. Based on the last observation, we conclude that these conditions were not suitable to execute the complete Ni-complex catalytic cycle. Therefore, guided by seminal reports by Ju,<sup>80</sup> Wickens<sup>68</sup> and Jui,<sup>81</sup> as well as, our previous experience in a generation of  $\text{CO}_2$  anion radical,<sup>62</sup> we modified reaction conditions introducing a photocatalyst (PC), like 4-CzIPN, and thiol **5aa** (mesna) to enhance the generation of the required XAT reagent through a thiy radical-aided HAT from the formate anion (Scheme 2, ent. 5). Additionally, we expected that generated under reaction conditions, PC-derived radical anion will also serve as a reductant for Ni(I) species to deliver Ni(0) to close the cross-coupling catalytic cycle. Now, an activation of substrate **1a** proceeded efficiently, but product **4a** still dominated. The yield of **3aa** did not exceed 15%. The replacement of 4-CzIPN by 4-DPAIPN and the use of other thiols than mesna resulted in a slight improvement only. This confirmed our previous suspicions about not efficient synchronicity of HAT and Ni-catalyzed cross-coupling steps; thus, we hypothesized that better synchronization of the reaction rates of individual processes should break the current impasse and significantly increase the efficiency of the process. Therefore, considering previous observations indicating that electrochemical conditions should enable the effective realization of the nickel catalytic cycle and the substrate **1a** activation strategy based on photoinduced-XAT, we decided to combine these strategies and investigate the possibility of alkenylation of compound **1a** with vinyl bromide **2a** under photoelectrochemical conditions.

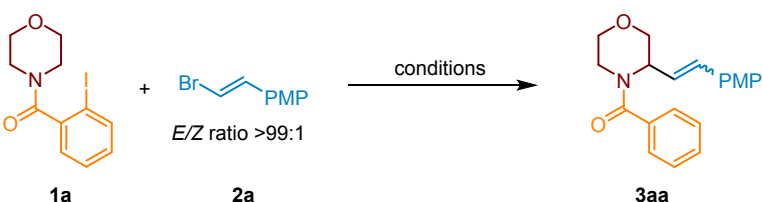
In initial photoelectrochemical experiments, the mixture of vinyl bromide **2a** and morpholine derivative **1a**, containing HCOOCs, thiol **5ab** and Ni-complex ( $\text{Ni}(\text{glyme})\text{Cl}_2 + \text{dtbbpy}$ ) in DMSO, was irradiated (395 nm) and electrolyzed (3 mA) for 12 h. The initial electrochemical setup consisted of an undivided electrochemical cell equipped with RVC and  $\text{Ni}(\text{foam})$  as anode and cathode, respectively. The  $\text{TBABF}_4$  was used as an electrolyte. Under these conditions, the expected product **3aa** was obtained in 35% yield (conversion of **1a** 89%) along with side product **4a** (Scheme 2, ent. 6d). This promising result encouraged us for further optimization of this process (Scheme 3).

We started the optimization of a photoelectrochemical protocol from examination of the influence of Ni salt on the products' yield. The replacement of  $\text{Ni}(\text{glyme})\text{Cl}_2$  by  $\text{Ni}(\text{glyme})\text{Br}_2$  allowed to



increase the product yield from 34% to 51% (Scheme 3, ent. 2). For other Ni salts, like  $\text{NiI}_2$ ,  $\text{Ni}(\text{OTf})_2$  or  $\text{Ni}(\text{cod})_2$ , the yields were much lower (see e-SI, §4.2.1.1). Next, we focused on the ligand choice. Initially 4,4'-di-*tert*-butyl-2,2'-bipyridine (dtbbpy) was used, however, further experiments demonstrated that the best results can be achieved when Ni-complex with PyBOX ligand was employed (Scheme 3, ent. 3 and e-SI, §4.2.1.2). Initially, 10 mol% loading of Ni salt and 11 mol% of PyBOX ligand was employed, however, we found out that these amounts can be lowered to 5 mol% and 5.5 mol%, respectively, without significant change of SM's conversion and product's yield after standard 12 hours. Further decrease of amount of Ni salt to 3 mol%, decreased conversion of **1a** from >99% to 67% and product yield to 53% after standard 12 h (see e-SI, §4.2.2.2).

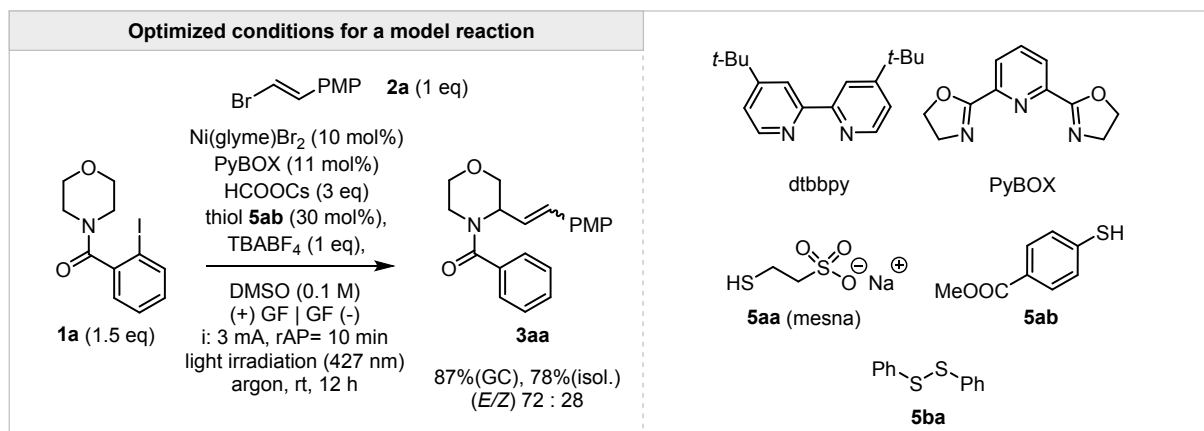
Article Online  
DOI: 10.1039/D5SC08559D



The modified parameter is marked in a color

Entry	Ni salt	ligand	formate salt	thiol	solvent	light	electrodes <sup>a</sup>	Conv. of <b>1a</b> <sup>b</sup>	Yield of <b>3aa</b> <sup>b</sup>	E/Z ratio
1.	$\text{Ni}(\text{glyme})\text{Cl}_2$	dtbbpy	HCOOCs	<b>5aa</b>	DMSO	395 nm	(+) RVC   $\text{Ni}_{\text{foam}}$ (-)	78%	6%	82 : 18
2.	$\text{Ni}(\text{glyme})\text{Br}_2$	dtbbpy	HCOOCs	<b>5aa</b>	DMSO	395 nm	(+) RVC   $\text{Ni}_{\text{foam}}$ (-)	89%	51%	96 : 04
3.	$\text{Ni}(\text{glyme})\text{Br}_2$	PyBOX	HCOOCs	<b>5ab</b>	DMSO	395 nm	(+) RVC   $\text{Ni}_{\text{foam}}$ (-)	>99%	67%	60 : 40
4.	$\text{Ni}(\text{glyme})\text{Br}_2$	dtbbpy	HCOOK	<b>5ab</b>	DMSO	395 nm	(+) RVC   $\text{Ni}_{\text{foam}}$ (-)	89%	51%	89 : 11
5.	$\text{Ni}(\text{glyme})\text{Br}_2$	PyBOX	HCOOCs	<b>5aa</b>	DMSO	395 nm	(+) RVC   $\text{Ni}_{\text{foam}}$ (-)	78%	6%	86 : 14
6.	$\text{Ni}(\text{glyme})\text{Br}_2$	dtbbpy	HCOOCs	<b>5ba</b>	DMSO	395 nm	(+) RVC   $\text{Ni}_{\text{foam}}$ (-)	>99%	51%	90 : 10
7.	$\text{Ni}(\text{glyme})\text{Br}_2$	PyBOX	HCOOCs	<b>5ab</b>	MeCN	395 nm	(+) RVC   $\text{Ni}_{\text{foam}}$ (-)	68%	9%	92 : 08
8.	$\text{Ni}(\text{glyme})\text{Br}_2$	PyBOX	HCOOCs	<b>5ab</b>	DMF	395 nm	(+) RVC   $\text{Ni}_{\text{foam}}$ (-)	63%	16%	93 : 07
9.	$\text{Ni}(\text{glyme})\text{Br}_2$	PyBOX	HCOOCs	<b>5ab</b>	DMSO	400 nm	(+) RVC   $\text{Ni}_{\text{foam}}$ (-)	>99%	38%	62 : 38
10.	$\text{Ni}(\text{glyme})\text{Br}_2$	PyBOX	HCOOCs	<b>5ab</b>	DMSO	427 nm	(+) RVC   $\text{Ni}_{\text{foam}}$ (-)	>99%	72%	65 : 35
11.	$\text{Ni}(\text{glyme})\text{Br}_2$	PyBOX	HCOOCs	<b>5ab</b>	DMSO	440 nm	(+) RVC   $\text{Ni}_{\text{foam}}$ (-)	>99%	56%	62 : 38
12.	$\text{Ni}(\text{glyme})\text{Br}_2$	PyBOX	HCOOCs	<b>5ab</b>	DMSO	395 nm	(+) RVC   RVC (-)	>99%	57%	59 : 41
13.	$\text{Ni}(\text{glyme})\text{Br}_2$	PyBOX	HCOOCs	<b>5ab</b>	DMSO	395 nm	(+) GRF   $\text{Ni}_{\text{foam}}$ (-)	>99%	42%	83 : 17
14.	$\text{Ni}(\text{glyme})\text{Br}_2$	PyBOX	HCOOCs	<b>5ab</b>	DMSO	395 nm	(+) GRF   GRF (-)	>99%	65% <sup>c</sup>	68 : 32
15.	$\text{Ni}(\text{glyme})\text{Br}_2$	PyBOX	HCOOCs	<b>5ab</b>	DMSO	427 nm	(+) GRF   GRF (-)	>99%	87% <sup>c</sup>	72 : 28

<sup>a</sup> current 3mA; <sup>b</sup> determined by GC; <sup>c</sup> with alternating electrode polarity over 10 min; RVC = reticulated vitreous carbon, GRF = graphite.



**Scheme 3.** Optimization studies on photoelectrochemical C-H alkenylation of amines (selected examples). PMP = 4-methoxyphenyl.

Among various formate salts,  $\text{HCOOCs}$  was the reagent of choice mostly due to the best solubility in DMSO in compare to other formats (see e-SI, §4.2.1.4). The conversions of **1a** in the presence of K, Na or Li formate were in range of 42–66 %, and only traces of product **3aa** were detected. Interestingly, tetrabutylammonium formate (HCOOTBA) allowed for complete conversion of **1a** but the yield of **3aa** was less than 40% of product, indicating that it affected the cross-coupling step (see e-SI, §4.2.1.4).

The initially mesna (**5aa**) was used as a HAT reagent. However, an examination of other thiols (see e-SI, §4.2.1.3) revealed that methyl 4-mercaptopbenzoate (**5ab**) provides complete conversion of **1a** and the highest yield of **3aa** (67%). Interestingly, its *ortho*-isomer delivered product **3aa** only in 37% (see e-SI, §4.2.1.3). In case of the electron-rich aromatic thiols (e.g., 4-mercaptopanisol) and aliphatic thiols (e.g. CySH or methyl mercaptoacetate) the yields of the model product did not exceed 20%, beside over 90% conversion of starting material **1a** (see e-SI, §4.2.1.3).

As already mentioned, DMSO resulted to be the solvent of choice which assure proper solubility of all reagents, including  $\text{TBABF}_4$  (1 equiv) which served as an electrolyte of choice (see e-SI, §4.2.1.5). The optimal concentration was 0.1 M with respect to substrate **1a**. Higher dilution (0.05 M) caused dramatic decrease of yield of **3aa** and increase content of reduced substrate (**4a**). In case of other solvents, like MeCN or DMF, a conversion of **1a** was ca. 60% (after 12 h), but the product's yield was <15%, indicating that these solvents strongly affect the cross-coupling step (Scheme 3, ent. 7 and 8) (see e-SI, §4.2.1.6). Furthermore, the solvent mixtures, like DMSO/water or DMSO/MeCN, were examined to improve the yield of the reaction, however, all of these attempts were not successful (see e-SI, §4.2.1.6).

Finally, we focus on an optimization of photochemical and electrochemical conditions. Initial conditions, a constant current electrolysis (3 mA) in the presence of an RVC anode and a Ni foam cathode along with purple light irradiation (395 nm) provided the product **3aa** in 67% yield (Scheme 3, ent. 3). The use of light sources with longer wavelength light resulted in a significant decrease of the product's yield, except in the experiment when blue light with a wavelength 427 nm was applied (ent. 3 and 9–11). In this case, the yield of the product increased up to 72% (ent. 10). The replacement of the RVC electrode by a graphite one resulted in a lower yield (ca. 42%, ent. 13). However, when two graphite electrodes were used instead of RVC and Ni(foam) ones, the model product was obtained in 65% (irradiation 395 nm) (ent. 14) and 87% (irradiation 427 nm) (ent. 15) yield. Additionally, we have also checked the influence of an applied current by varying it from 1 to 4 mA (see e-SI, §4.2.3.2). The current of 3 mA was optimal.

During optimization studies, we found out that with the efficiency of the cross-coupling process decreased during the experiments due to “poisoning” of the anode by deposition of solid by-products at the electrode surface. To avoid this, we set up a power supply to change periodically the polarization of the electrodes. We examined different polarization changing times, 5, 10, 15 min, and the 10 min intervals were optimal (3 mA for 10 min then –3 mA for 10 min). The alternating current electrolysis<sup>82</sup> with time intervals less than 60 s was ineffective, and the target product was obtained in yields below 65%. Therefore, irradiation with purple light (395 nm), and electrolysis with polarization change of two

graphite electrodes every 10 min resulted in an increase of the product yield up to 65% (Scheme 3, entry 14). Finally, the change of a light wavelength from 395 nm to 427 nm, allowed for further improvement of the process and yielded the product **3aa** in 87%.

Finally, among 2-halobenzamides, the iodo-derivative, e.g., **1a**, demonstrated superior reactivity and efficiency of the alkenylation process (see e-SI, §4.3.1). In the context of vinyl halides, vinyl bromide **2a** emerged as the superior cross-coupling partner, owing to its exceptional combination of stability and reactivity (see e-SI, §4.3.2).

The final optimization studies were devoted to elaborate the optimal amounts of the required reagents. Thus, the reaction of **1a** and **2a** in a ratio of 1:1.5, in the presence of 1 equiv. of TBABF<sub>4</sub>, 3 equiv. of HCOOCs, 30 mol% of thiol **5ab**, 10 mol% of Ni(glyme)Br<sub>2</sub>, and 11 mol% of PyBox ligand in DMSO (0.1 M) yielded product **3aa** in 87% (GC) as a mixture of *E/Z* isomers in a ratio 72:28 (Scheme 3). Aqueous work-up of the post-reaction mixture followed by flash column chromatography delivered **3aa** in 78% isolated yield.

**Substrates' scope.** With optimal conditions in hand, we next explored the scope of the aryl radical-triggered remote C(sp<sup>3</sup>)-H alkenylation protocol with various heterocyclic scaffolds and model vinyl bromide **2a**. As shown in Scheme 4, C-H alkenylation of a range of 2-iodobenzoyl-protected saturated heterocycles with different ring size proceeded smoothly and provided the desired products (e.g., **3ab**, **3al** and **3aq**) smoothly in 72-75% isolated yield. On the contrary, alkenylation of the azetidine ring failed (**3as**), and deiodinated azetidine benzamide was obtained as a single product, indicating that the geometry of the 4-membered ring along with its rigidity does not allow for executing the 1,5-HAT process since the distance between radical center and ring's hydrogen atom is too long.

Additional heteroatoms in the ring, like oxygen for **1a** and **1g** or nitrogen in the case of **1d**, **1e** derivatives, did not have a significant influence, and desired products **3aa**, **3ag**, **3ad** and **3ae**, respectively, were obtained in very good yields. Only in the case of alkenylation of thiomorpholine-based benzamide **1c**, the desired product **3ac** was isolated in lower yield (55%), although the starting material was consumed completely. The product **3ac** was accompanied with an increased amount of deiodinated starting material (~20-30%), indicating potent issue either with the HAT process. We believe that it could be the effect of a change of the 6-membered ring geometry in thiomorpholine due to the presence of the S atom and elongation of the C-S bonds lengths compared to C-C (like for piperidine) or C-O (like for morpholine) that may affect the 1,5-HAT transition state geometry decreasing the efficiency of the H-atom translocation. Of course, the alternate negative interactions of S atom with Ni-catalyst, which might affect the cross-coupling cycle, cannot be neglected too.

Notably, an alkenylation of monocyclic 6-membered substrates usually underwent more efficiently than for the corresponding fused analogues (e.g., **3aa** vs. **3ak** or **3ab** vs. **3ah**), which often were accompanied by a side benzamide product originating from a deiodination of starting 2-iodobenzamide. However, at the same time, all benzofused products (e.g., **3ah**, **3ak**, etc.) were formed exclusively as *E*-isomers, whereas for monocyclic substrates the content of (*Z*)-isomer varied from 2 up to 30%. A potent rationalization of this phenomenon relates to a different conformational dynamic of

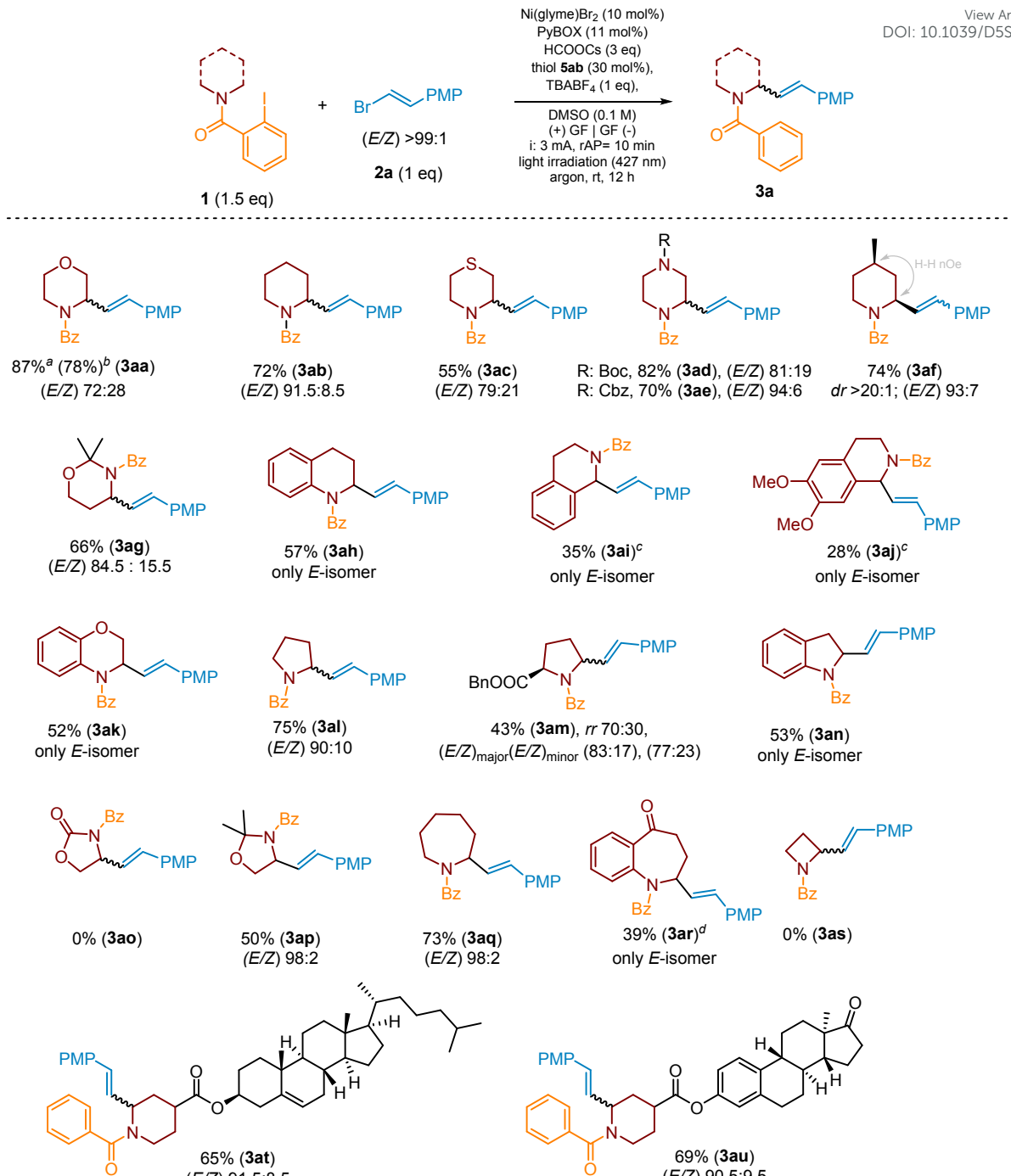


mono-cyclic and fused heterocyclic scaffolds. It should be expected that reducing the degrees of freedom in fused systems should significantly reduce their conformational dynamics, which will potentially translate into more difficulty obtaining the appropriate geometry of the transition state of the HAT process. As a result, the rate of the H-atom transfer should decrease, thus providing an opportunity for competitive quenching of the aryl radical to form the corresponding benzamide, which is in accordance with our experimental observations.

For heterocyclic substrates, such as **1i** and **1j**, with two potent positions for an H-atom abstraction, the regioselectivity of the HAT reaction was governed by the relative stability of the resulting  $\alpha$ -aminoalkyl radical. As presented in Scheme 4, in these cases, the 1,5-HAT step proceeded regioselectively at the C-1 position, resulting in the formation of more stable benzyl-type radical species, and yielded products **3ai** and **3aj**, respectively. Disappointingly, in both cases the yields did not exceed 40% due to the high content of unwanted deiodinated side benzamides (40-60%).

A significance of conformational factors was also strongly manifested in a C-H functionalization of the 5- and 7-membered substrates. As previously, the alkenylation of 5-membered pyrrolidine ring (**1l**) proceeded more efficiently than for the fused analogue, indolidine (**3al** vs. **3an**). Furthermore, a flat nature of an oxazolidinone ring (e.g., **3ao**) along with a specific arrangement of the benzoyl group makes the effective orientation of the HAT directing group strongly disfavoured due to an electric repulsion and a steric hindrance. As a result, the XAT-generated aryl radical species is incapable of an abstraction of any hydrogen atom, and is quenched directly, yielding *N*-benzoylated oxazolidinone only. The replacement of a carbonyl group in the oxazolidinone ring (**1o**) by a  $C(sp^3)$ -atom (oxazoline **1p**) increased conformational lability of the ring enabling the 1,5-HAT process and yielding compound **3ap** in 50% yield (isol.). Nevertheless, the flexibility of the oxazoline 5-membered ring is still not enough to reach the efficient geometry of the HAT-transition state, in compare with 6-membered heterocycles; therefore, again, desired product **3ap** was accompanied by a type-**4** side product. Herein, the high ring lability along with entropic factors which decrease the probability of the system to adopt the optimal geometry of the HAT-transition state that again results in a decrease of the rate of an H-atom abstraction promoting side quenching of aryl radical species.





<sup>a</sup> yields assigned by GC with an internal standard, (E/Z) ratio assigned by <sup>1</sup>H NMR or GC; <sup>b</sup> isolated yield; <sup>c</sup> conv. 50% of benzamide after 12 h; <sup>d</sup> along with deiodinated starting material (ca. 20%). rr = regioisomers' ratio; PMP = 4-methoxyphenyl

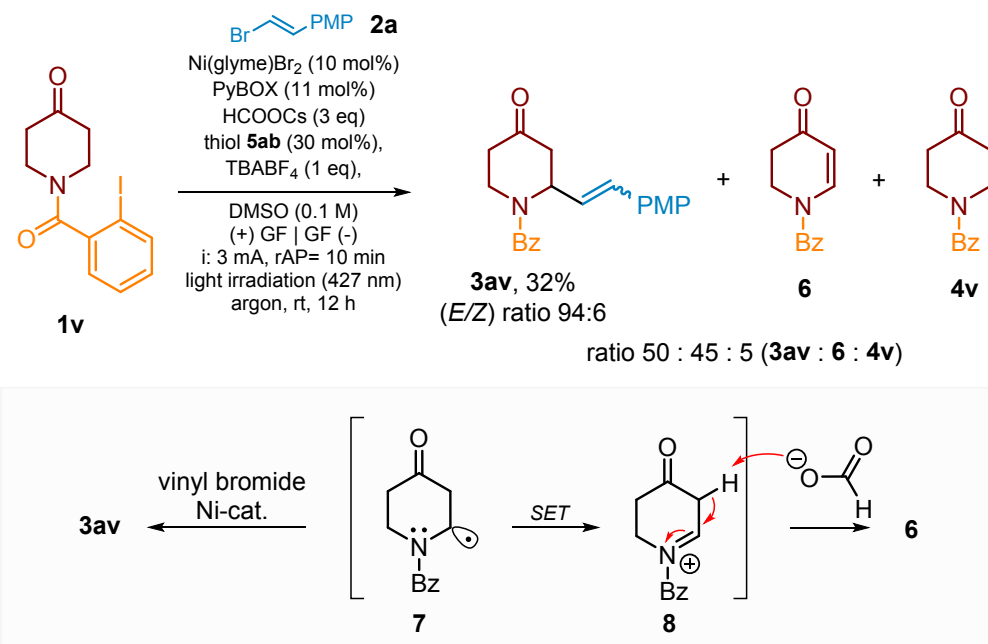
**Scheme 4.** The scope amines for remote  $\alpha$ -C(sp<sup>3</sup>)-H alkenylation of heterocycles **1**.

In the case of an alkenylation of benzoazepan-5-one derivative **1r** (product **3ar**), the initial steps, a generation of an aryl radical and the subsequent 1,5-HAT process, proceeded noticeably slower than for azepane derivative **1q**, as well as other heterocyclic substrates. As a result, after standard 12 h, product **3ar** was isolated in 39%, only, and was accompanied by dehalogenated substrate (ca. 20%) and numerous vinyl bromide homo-coupling products. Additionally, ca. 10-15% of unreacted substrate



**1r** was recovered. The reaction proceeded well also for more complex amines, like **estrone**<sup>82</sup> and cholesterol-derived substrates, delivering products **3at** and **3au** in good yields and high content of *E*-isomer (Scheme 4). In both cases single diastereoisomer was isolated, however, overlapping of diagnostic signals in NMR spectra did not allow to assign clearly relative configuration.

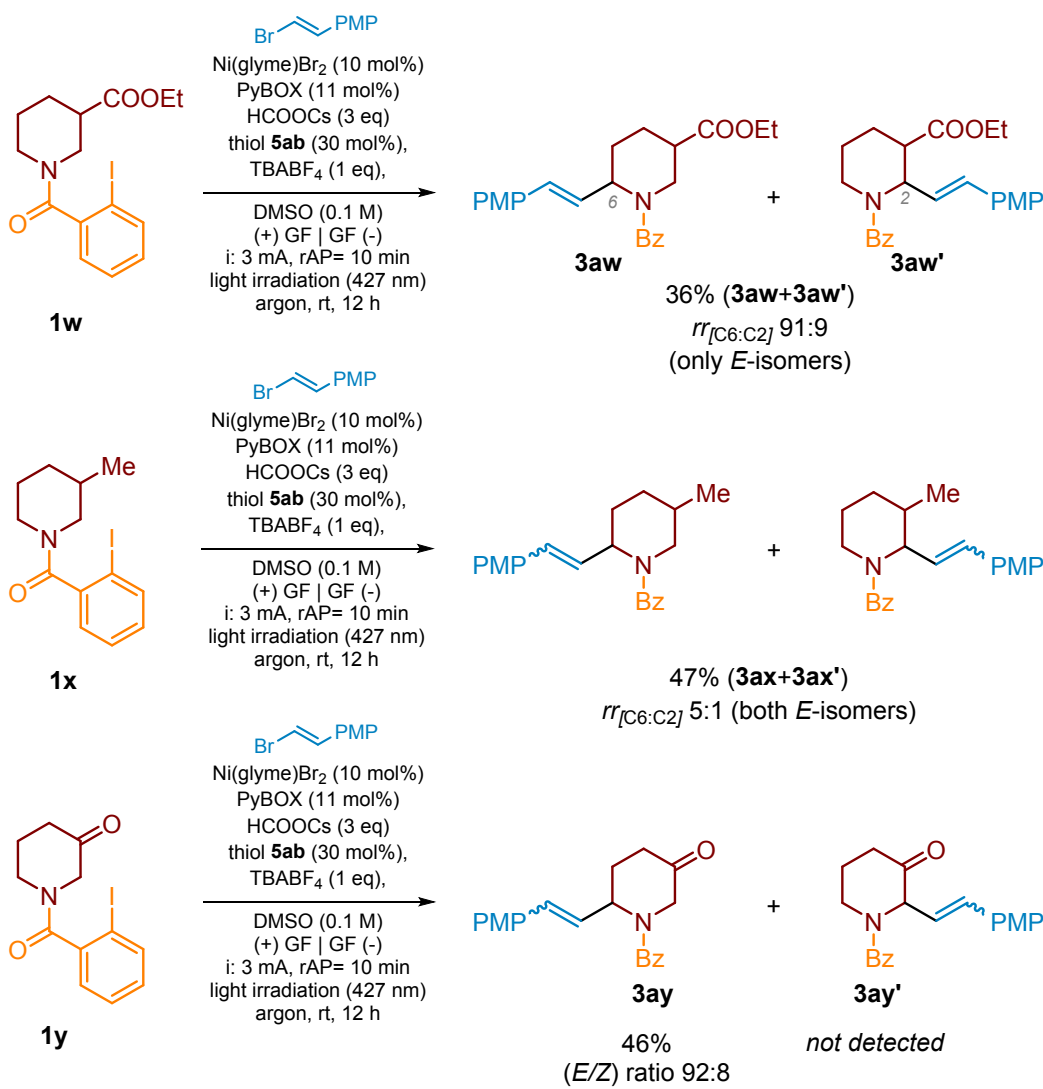
Ring substituted heterocycles, e.g., 4-methylpiperidine **1f**, are also suitable substrates for C-H alkenylation process, as demonstrated in Scheme 4, and for example, product **3af** was yielded in 74%. An intriguing substrate was piperidin-4-one derivative **1v**. Under standard conditions, beside expected product **3av** (yield 32%), its alkenylation also delivered compound **6** (yield 30%) and a small amount of side-product **4v** (Scheme 5). The product **6** plausibly originated from an oxidation of  $\alpha$ -aminoalkyl radical intermediate **7** to the corresponding iminium cation **8** followed by a subsequent base-mediated deprotonation (e.g., by formate anion) at the C $\alpha$ -position to the carbonyl group to deliver enamide **6**. Recently, Yatham and co-workers<sup>83</sup> demonstrated synthesis type-**6** cyclic enamides in closely related approach involving the radical translocation followed by the Co-assisted dehydrogenation.



**Scheme 5.** The C-H alkenylation of piperidin-4-one derived benzamide **1v**. PMP = 4-methoxyphenyl.

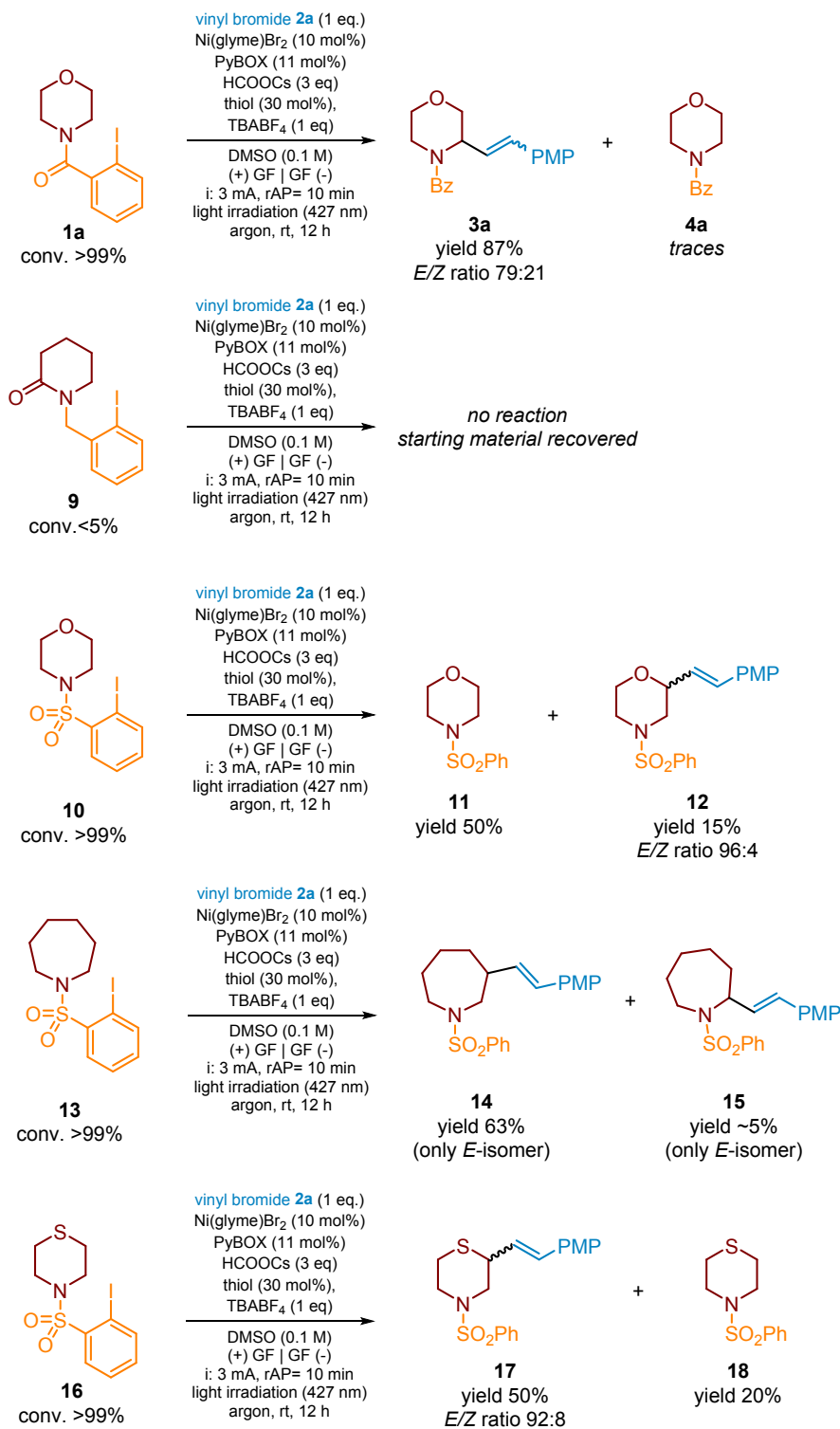
We expected that type **6** enamide could also be formed during an alkenylation of substrate **1w**, bearing ester functionality at the C3 position. However, it was not a case, and such product was not detected in the reaction mixture. On the other hand, this reaction led to the formation of two regioisomeric (*E*)-products **3aw** and **3aw'**, in a ratio of 91:9 (Scheme 6). The NMR analysis of the crude reaction mixture revealed only traces of (*Z*)-isomers (<5%). We were not able to separate both regioisomers to confirm the relative configuration. The regioisomeric mixture was also obtained for an alkenylation of 3-methyl-substituted substrate **1x** (Scheme 6, **3ax/3ax'** in a ratio of 5:1) Again, the C6-alkenylated product was the major one, and only traces of the corresponding (*Z*)-isomers were noticed by a <sup>1</sup>H NMR analysis.

On the contrary, piperidin-3-one **1y** derivative delivered only C6-alkenylated products **3ay** (*E/Z*-isomers) mixture in a ratio of 92:8) in a moderate yield of 46%. For all these cases lower products yields were the effect of side substrate reduction leading to the corresponding benzamides.



**Scheme 6.** Remote C-H alkenylation of 3-substituted piperidine scaffolds. The *E/Z* ratio of vinyl bromide **2a** was >99:1. PMP = 4-methoxyphenyl.





**Scheme 7 .** The effect of a HAT-directing group on C-H alkenylation of morpholine derivatives with vinyl bromide **2a**.

Next, using a model morpholine scaffold (Scheme 7), we investigated the scope of a HAT directing group capable of promoting a 1,5-HAT reaction. The 2-iodobenzoyl group excelled the other two examined functional groups, 2-iodobenzyl and 2-iodobenzosulfonyl, in terms of effective radical translocation through the 1,5-HAT reaction. The 2-iodobenzyl group was completely worthless since it



did not deliver an aryl radical through XAT by the  $\text{CO}_2^-$ , under standard reaction conditions. Neither the expected product nor the deiodinated side-product, *N*-benzyl morpholine, were detected in the crude reaction mixtures by the MS analysis. Consequently, only about all of the starting material **9** could be recovered from these experiments. This led us to conclusion that electron-deficient character of the HAT directing group is essential for an efficient cleavage of the  $\text{C}(\text{sp}^2)\text{-I}$  bond by an XAT reagent.

Open Access Article. Published on 21 January 2026. Downloaded on 1/25/2026 3:10:21 AM.  
This article is licensed under a Creative Commons Attribution-NonCommercial 3.0 Unported Licence.  
DOI: 10.1039/D5SC08559D

The reaction of 2-iodobenzosulfonamide **10** delivered primarily deiodinated product **11** (~50%) (Scheme 7). We have also isolated a small quantity of another compound. Its structure was elucidated and indisputably assigned as **12**, according to NMR spectra, including COSY and HSQC correlations (see e-SI). An installation of alkenyl fragment at the C3 position of the morpholine ring indicated that initial H-atom translocation proceeded in the 1,6-manner in contrary to all so far studied examples. It is well known that thanks to the longer length of  $\text{N-SO}_2$  and  $\text{C-SO}_2$  bonds, sulfamides are capable of promoting 1,6- over 1,5-HAT in acyclic systems.<sup>39, 41, 44, 84-87</sup> However, according to our best knowledge, it is the first example of such  $\beta\text{-C}(\text{sp}^3)\text{-H}$  functionalization for the heterocyclic substrate. The low yield of product **12** (~15%, (*E/Z*)-isomers mixture in a ratio of 96:4) with a simultaneous large content of side-product **11** in the reaction mixture is not surprising considering that the 1,6-HAT process proceeds through a 7-membered transition state and the 6-membered structure of the substrate with its conformational preferences should definitely not favour efficient translocation of the H atom. At this point, we hypothesized that increasing the substrates' ring size should facilitate the 1,6-HAT process thanks to the higher flexibility of such rings. Therefore, to prove such assumption, we prepared azepane benzosulfamide **13** and subjected it to the reaction with model vinyl bromide **2a** under standard photoelectrochemical conditions. As expected, the reaction proceeded with complete conversion of substrate **13** and yielded compound **14** (only *E*-isomer) in 63%. Notably, deepen analysis of the crude reaction mixture revealed the presence of small quantities of the 1,5-HAT-derived product **15** but its yield did not exceed 5%.

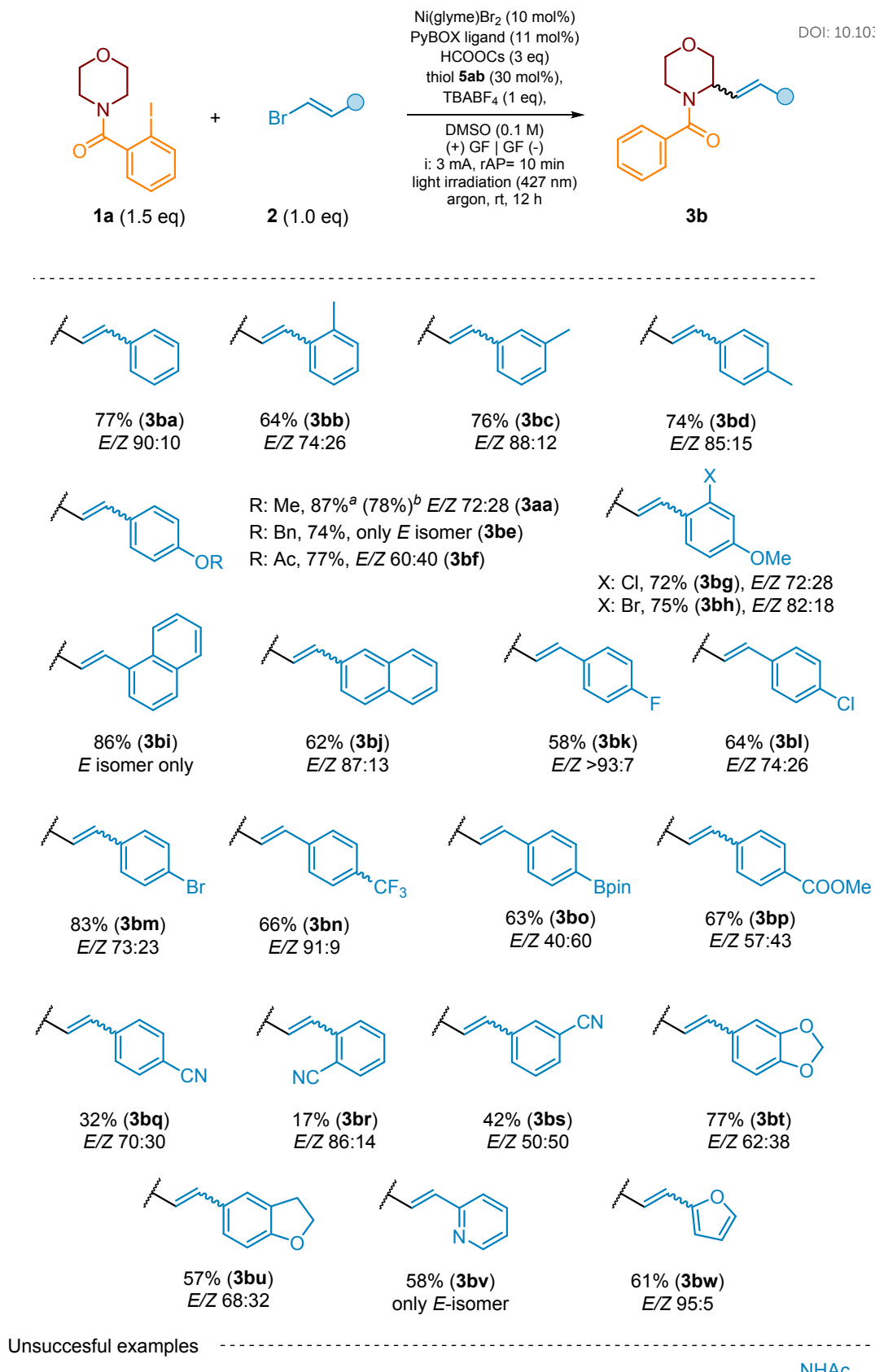
The above-presented results encouraged us for one more experiment. As already mentioned, among 6-membered heterocycles, the  $\alpha\text{-C-H}$  alkenylation of the thiomorpholine ring proceeded in a moderate yield (Scheme 4, **3ac** vs. **3aa**, **3ab**, **3ad-3af**), which was rationalized by a deformation of the 6-membered ring due to the longer length of the C-S bond. On the other side,  $\beta\text{-C-H}$  alkenylation of morpholine scaffolds assisted by the 2-iodobenzosulfonyl group yielded product **12** poorly. Therefore, we hypothesized that the replacement of the HAT directing group in the thiomorpholine ring and the combination of both structural effects connected with the presence of the S-atom should enhance the HAT process along with a change of regioselectivity of the C-H functionalization. Indeed, the C-H alkenylation of substrate **16** with model vinyl bromide **2a** yielded expected product **17** in 50% along with side product **18** (20%). The increase in yield from 15% for substrate **12** to 50% for product **17** confirmed the above assumption; however, the enhancement of HAT is moderate, indicating that the geometry of the transition state is still not the most efficient one.

Subsequently, we investigated the scope of the vinyl bromides in the reaction with morpholine-derived substrate **1a**. The reaction proceeded smoothly for a range of 2-aryl-substituted vinyl bromides bearing both electron-donating and electron-withdrawing groups, indicating very good functional group

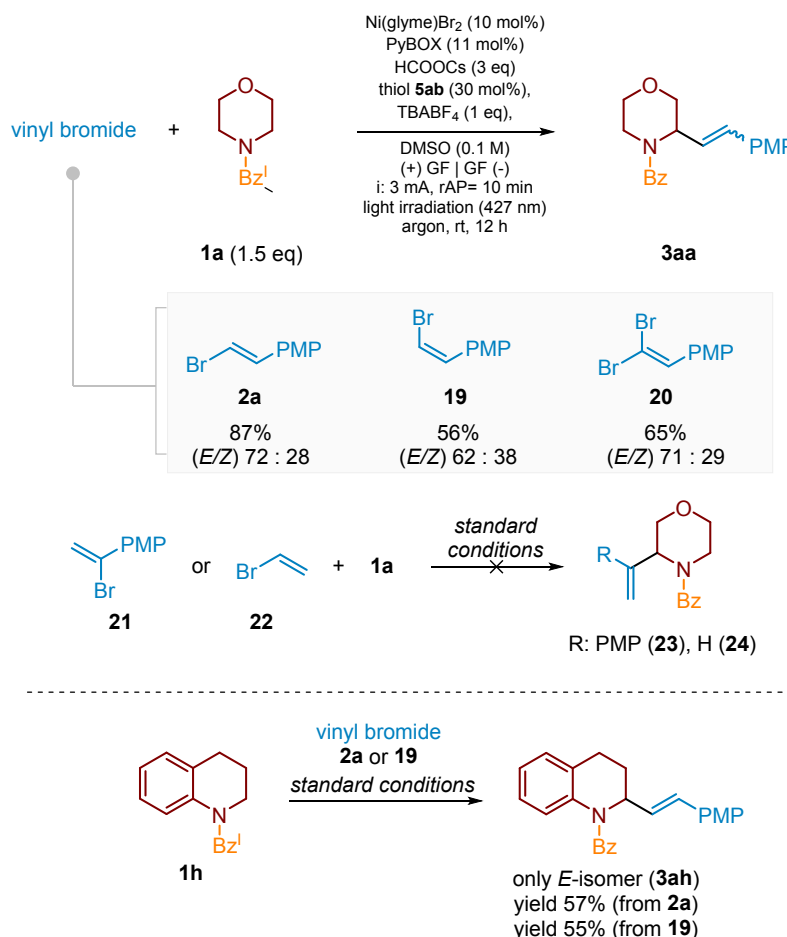
tolerance (Scheme 8). 2-Aryl vinyl bromides with a nitro group at the phenyl ring did not provide the expected product, plausibly due to potent photoexcitation of the nitro group<sup>88-91</sup> followed by side reactions. The cross-coupling of 2-aryl vinyl bromides with a CN group at various positions of phenyl (**2v-2x**) proceeded less efficiently (products **3bq-3bs**) than for other EWG groups, like ester ones (e.g., **2u**) which yielded product **3bp** in 67%. The reason of that were competitive side radical reactions of CN group as a radical acceptor,<sup>92, 93</sup> resulting in low yield of the desired products and complicated product reaction mixture.

We were delighted to find that 2-aryl vinyl bromide with a boronic acid ester group can also be efficiently coupled with a morpholine ring (63%), providing product **3bo** for further functionalization via standard cross-coupling reactions. Finally, we examined the reactivity of several vinyl bromides bearing heterocyclic rings (**2y-2ab**). As seen in Scheme 8, these reagents were also suitable cross-coupling partners for the investigated reaction sequence, providing desired products (**3bt-3bw**) in 58-77% yield.



<sup>a</sup> determined by GC; <sup>b</sup> isolated yield.

**Scheme 8.** The scope vinyl bromides for remote C(sp<sup>3</sup>)-H alkenylation of saturated heterocycles. View Article Online DOI: 10.1039/D5SC08559D  
For the E/Z ratio for starting vinyl bromides please see e-SI, §3.2).



**Scheme 9.** Reactivity of isomeric vinyl bromides. The E/Z ratio >99:1 for vinyl bromide **2a** and 1:17.5 for vinyl bromide **19**. PMP = 4-methoxyphenyl

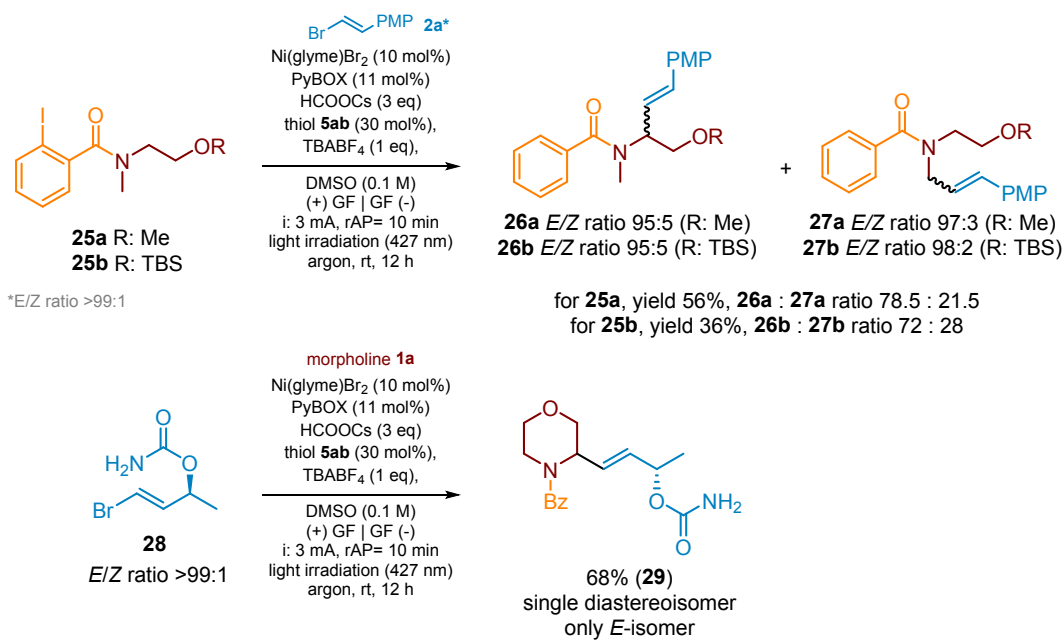
In addition to (*E*)-vinyl bromides (**2**), their (*Z*)-isomers (e.g., **19**) may also be used in the examined alkenylation procedure. Scheme 9 presents that for both vinyl bromides, **2a** and **19**, the product **3aa** was obtained as an (*E/Z*)-isomers mixture, with the (*E*)-isomer predominating. However, in the case of the (*Z*)-isomer, the cross-coupling proceeded relatively slower, delivering product **3aa** in lower yield after the standard reaction time (12 h). As already mentioned, in contrast to monocyclic amines, the C-H alkenylation of bicyclic heterocycles leads to (*E*)-products only, suggesting that steric effects might prevent subsequent *E*-to-*Z* isomerization. Such assumption seems to be supported by other experimental observation presented in Scheme 9. An alkenylation of quinolidine derivative **1h** with (*E*)-vinyl bromide **2a** yielded product **3ah** in 57% as a single (*E*)-isomer. An analogue reaction of **1h** with (*Z*)-vinyl bromide **19**, proceeded in slight less efficiently (yield 50%) but delivered the same (*E*)-isomer **3ah**.

Furthermore, vinyl dibromides, e.g., **20**, which served as intermediates in the synthesis of type-2 substrates, were also suitable for the investigated C-H functionalization, and delivered the product **3aa** again with dominance of the (*E*)-isomer after the subsequent debromination process under the same



reaction conditions. Disappointingly, in contrast to the 2-aryl vinyl bromides presented so far, their sterically more hindered 1-aryl substituted analogues, such as compound **21**, were much less efficient cross-coupling partners, and only traces of the desired products (e.g., **23**). The major product was dehalogenated morpholine benzamide **4a**. In addition, an alkenylation of the model substrate **1a** with unsubstituted vinyl bromide **22** was unsuccessful and did not furnish the desired 2-vinylated morpholine **24**.

The developed protocol could also be successfully applied for acyclic amine derivatives, like compounds **25a** and **25b** (Scheme 10). For both cases, an alkenylation with the model vinyl bromide **2a** delivered regioisomeric products **26** and **27** in 56% and 36% yield, respectively. Regiosomers **26a** and **26b** were major products indicating that 1,5-HAT toward the formation more stable of secondary  $\alpha$ -aminoalkyl radical is more preferred. Furthermore, so far used 2-aryl vinyl bromides could be replaced by their alkyl-substituted ones. The reactions with simple 2-alkyl vinyl bromides (see e-SI, §7), under standard reaction conditions, were unsuccessful since, in these cases, the rates of side debromination and homocross-coupling reactions were higher than desired XAT/HAT/cross-coupling sequence. The better results were achieved in case of more complex vinyl bromides, like compound **28**. The alkenylation of morpholine derivative **1a** with this bromide, under standard conditions, yielded product **29** in 68% as a single diastereoisomer and with (*E*)-geometry of a double bond, as presented in Scheme 10.



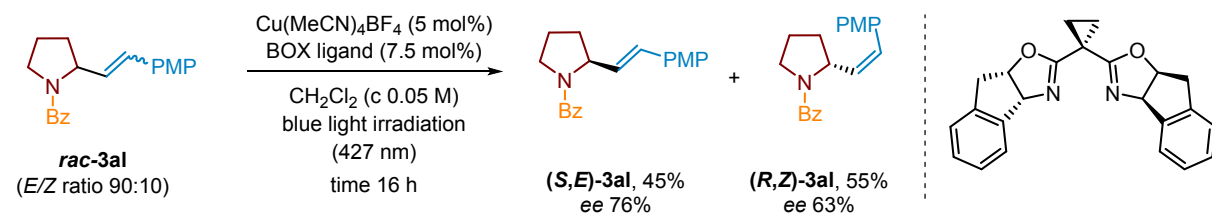
**Scheme 10.** Remote C-H alkenylation of acyclic amines and alkenylation with 2-alkyl substituted vinyl bromides.

Finally, we questioned whether the disclosed procedure could be done in an enantioselective manner by employing chiral Ni complexes. For this purpose, we replaced so far used PyBOX ligand by its chiral analogues, and attempted to perform the reaction between morpholine **1a** and vinyl bromide **2a**. However, since we could not achieve suitable separation of all isomeric products **3aa** during HPLC



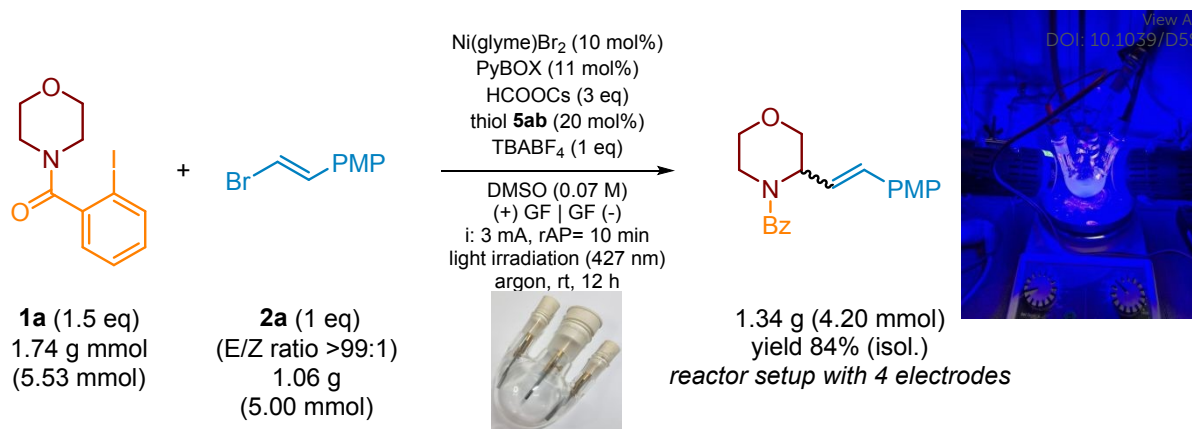
analysis of the racemic sample, we replaced the model substrate **1a** by pyrrolidine derivative **1I** which was then submitted to the alkenylation with vinyl bromide **2a**. Unfortunately, beside numerous chiral PyBOX ligands, we did not observe any asymmetric induction, resulting in a formation of the racemic (*E*)- and (*Z*)-products **3al**, although, the overall yields were quite high in all studied cases (see e-SI, §10). The same result was obtained when PyBOX ligands were replaced by a series of chiral BOX ligands (see e-SI, §10).

Contrarily to unsuccessful realization of enantioselective mode of C-H alkenylation, we focused on photochemical Cu complex-assisted kinetic resolution following the report by Yuan and Yu.<sup>94</sup> Under reported conditions, racemic pyrrolidine **3al** (*E/Z* mixture in ratio of 90:10), in the presence of chiral Cu-BOX ligand and under blue light irradiation (427 nm), yielded (*S,E*)-**3al** and (*R,Z*)-**3al** in 45% and 55%, respectively (Scheme 11). Enantiomeric excess for (*S,E*)-**3al** was 76%, whereas the optical purity of (*R,Z*)-**3al** was 63% ee.



**Scheme 11.** Photochemical kinetic resolution of pyrrolidine derivative **rac-3al** (*E/Z* ratio 90:10) in the presence of the chiral Cu/BOX complex.

**Applications.** To explore the practicality of this reaction, a scale-up experiment was carried out under the standard reaction conditions. Initially a reaction of **1a** and **2a** was performed in a 50-mL 3-neck round-bottom flask with angled side arms, however, the desired product **3aa** was obtained in a significantly lower yield (57%, 0.86 g starting from 1.0 g (4.7 mmol) of substrate **2a**) in compare to the same process at the 0.6 mmol scale (see e-SI, §12, Fig. SI-25). The change of reactor into 3-neck round-bottom flask with parallel side arms enhanced the yield to 61%. Finally, a placing additional to electrodes allowed to obtained 1.34 g (84%) of the desired product **3aa** (*E/Z* isomers ratio 90:10), starting from 1.06 g (5.00 mmol) of vinyl bromide **2a** and 1.74 g (5.53 mmol) of morpholine derivative **1a**.

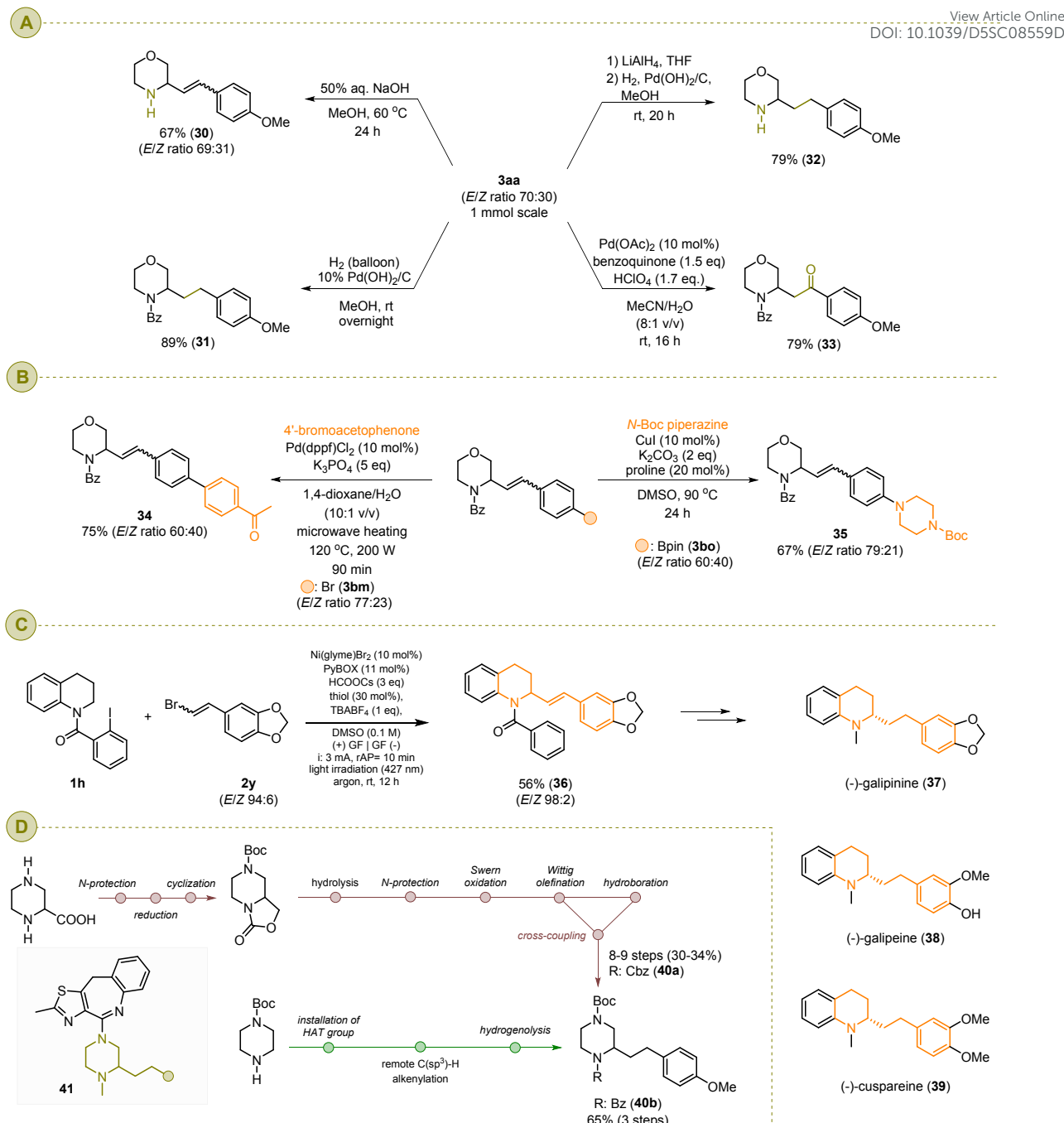


**Scheme 12.** A large-scale synthesis of compound **3aa**.

To demonstrate the synthetic potential of the alkenylated heterocycles prepared via our remote C(sp<sup>3</sup>)-H alkenylation conditions, model product **3aa** was subjected to several transformations presented in Scheme 13a. The basic hydrolysis of **3aa** yielded free amine **30** in 67%, its hydrogenation in the presence of Pd(OH)<sub>2</sub>/C yielded product **31** in 89%. Finally, a sequential reduction of amide functionality and hydrogenation of a double bond allowed for synthesis of morpholine **32** in 79% isolated overall yield. The Wacker oxidation of **3aa** delivered ketone **33** in 79%.

The tolerance of the functional group, like halides or boronic acid, makes an extraordinary opportunity to use the resulting products for their late-stage functionalization to deliver complex molecular systems. For example, boronic acid ester **3bo** was readily coupled with aryl halides, like 4'-bromoacetophenone, to furnish product **34** in 75% yield, as demonstrated in Scheme 13B. Notably, varying the aryl halides allows for a late-stage structure diversification of the core fragment, e.g., **1** and **3**, delivering a broad library of products, for instance, for structure-activity relation studies (SARS), a relatively faster and efficient way avoiding time-consuming parallel multistep synthesis. Furthermore, as presented in Scheme 13b, substrate **3bm** can be decorated by an additional heterocyclic scaffold through a Cu-catalyzed Ullmann-type coupling reaction with *N*-nucleophile, e.g., *N*-Boc piperazine, yielding product **35** in 67%.





**Scheme 13.** Synthetic application: (A) functional group transformations; (B) post-functionalization of type-3 products; (C) synthesis of galipinine precursor **36**; (D) Synthetic approach for the preparation of piperazine fragment of type-41 bioactive molecules

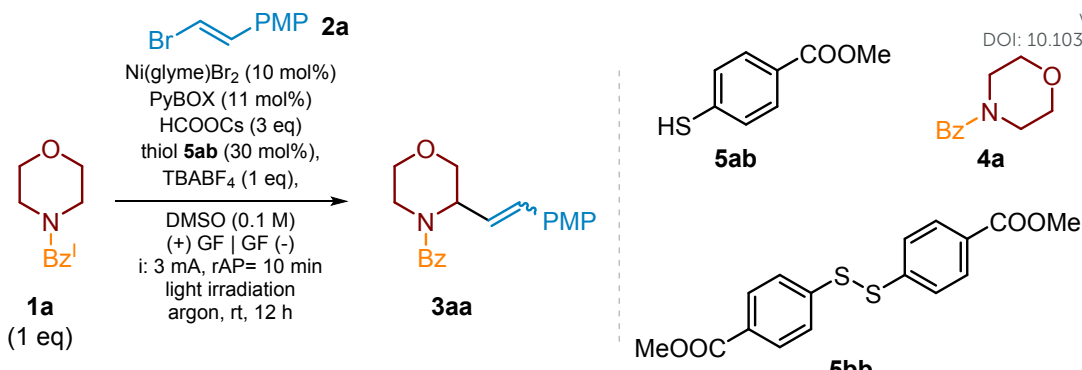
Another example of practical application of our alkenylation protocol is the synthesis of compound **36**, which can serve as a precursor of (-)-galipinine **37** (Scheme 13c). The same approach allows for construction of similar tetrahydroquinoline-based alkaloids, like (-)-galipeine **38** and (-)-cuspaine **39**. All of them are isolated from *Galipea officinalis* shrubby tree, whose trunk bark is used in the indigenous folk medicine for its healing properties.<sup>6</sup>



Moreover, as already presented in Scheme 4 and Scheme 8, a broad substrate scope regarding the vinyl bromides, as well as heterocyclic scaffolds, makes our protocol a suitable synthetic tool for rapid and efficient structure diversification either by the already mentioned post-functionalization or by varying both starting materials to differentiate either the heterocyclic core or the side chain. We demonstrated this by synthesizing the piperazine-containing compound **40b**. Such functionalized piperazine-based structural motif can be found in numerous naturally occurring compounds or drug candidates,<sup>95-98</sup> like type-**41** compounds widely investigated as a potent dopamine receptor antagonist for the treatment of psychotic disorders.<sup>99-102</sup> As shown in Scheme 13d, the already known approach for the synthesis of the core fragment, like compound **40a**, was executed in 8-9 steps starting from piperazine-2-carboxylic acid and in overall yield 30-33%.<sup>99</sup> No doubt, practical application of this reaction sequence for the preparation of the large library of type-**40a** structures, for instance, for SARS studies, is highly time-consuming what limits its synthetic value. Therefore, we proposed the synthesis analogue of **40a**, piperazine **40b** (R: Cbz), from readily available mono-protected piperazine, and included an installation of the HAT directing group, key C(sp<sup>3</sup>)-H alkenylation of the heterocyclic ring, and hydrogenation of the double bond. The target product, **40b**, was obtained in 65% overall yield.

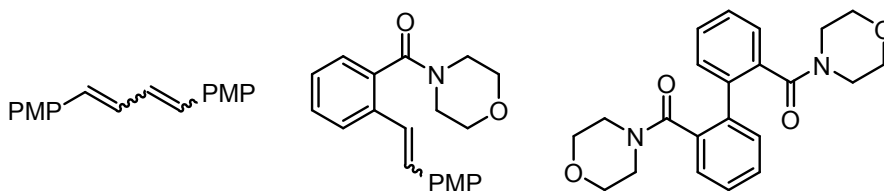
**Mechanism discussion.** To determine the essential parameters of the investigated process, we conducted several control experiments disclosed in Scheme 14.





Ent.	Deviation from optimal conditions	Conv. of <b>1a</b> <sup>a</sup>	Yield of <b>3aa</b> <sup>a</sup>	E/Z ratio
1.	none	>99%	87%	72:28
2.	without light irradiation	>90% <sup>b</sup>	5%	-
3.	without electrolysis (@ 427 nm)	>99% <sup>b</sup>	0%	-
4.	without electrolysis (@ 395 nm)	>90% <sup>b</sup>	>10%	-
5.	without HCOOCs (@ 395 nm)	54% <sup>b</sup>	0%	-
6.	without thiol (@ 427 nm)	38% <sup>b</sup>	6%	80:20
7.	without thiol (@ 395 nm)	75% <sup>b</sup>	6%	79:21
8.	without thiol and formate (@395)	25% <sup>b</sup>	0%	-
9.	disulfide <b>5bb</b> instead of <b>5ab</b> (@ 395 nm)	>99%	51%	80:20
10.	without argon	>99%	70%	87:13
11.	non-anhydrous DMSO & HCOOCs·H <sub>2</sub> O	87%	22-28%	-
12.	benzamide <b>4a</b> instead of <b>1a</b>	no reaction	-	-

<sup>a</sup> determined by GC analysis; <sup>b</sup> homocoupling and cross-coupling products assigned by MS:



Bz<sup>I</sup> = 2-iodobenzoyl; PMP = 4-methoxyphenyl

**Scheme 14.** Mechanism studies: the exclusion tests and control experiments.

In the absence of irradiation (Scheme 14, ent. 2), only traces of product **3aa** were noticed (~5%) although, the conversion of **1a** was above 90% due to side processes, like homo-coupling of **1a**, cross-coupling of **1a** with **2a** (Scheme 14, bottom), along with slight amounts of dehalogenated substrate (**4a**). These observations allowed us to draw two conclusions. Firstly, the Ni-catalyzed coupling step does not depend on photochemical conditions. Moreover, since only a catalytic amount of Ni salt is used (10 mol%), the formation of the mentioned by-products proves that electrochemical conditions ensure closure of the Ni-catalytic cycle, restoring of key Ni<sup>(0)</sup> species. Secondly, a light is plausibly essential to execute an activation of the substrate, e.g., **1a**, via HAT process.



Without electric current, only traces of product **3aa**, as well as, homo/cross-coupling side products, were detected along with dominant side-product **4a** (Scheme 14, ent. 3 and 4) regardless whether a blue (427 nm) or a purple light (395 nm) was applied. This observation supported the above statement about essential role of electrolysis on a cross-coupling cycle.

In the control experiment conducted without the addition of formate salt, the conversion of substrate **1a** proceeded very slowly, reaching only 9% after 8 hours. The reaction predominantly yielded homo- and cross-coupling products, as detected by mass spectrometry (Scheme 14, ent. 5). Furthermore, the formation of side product **4a** did not exceed 5-7% even after 12 hours. These results highlight the pivotal role of formate in activating the starting material and demonstrate the absence of other reactive species in the reaction mixture capable of reducing the  $C(sp^2)-I$  bond.

When the model reaction was performed without thiol **5ab** under a blue light irradiation (427 nm, ent. 6) only 38% conversion of substrate **1a** was noticed along with a slight amount of product (6%, *E/Z* 80:20). On the other side, when a light wavelength was change from 427 to 395 nm (ent. 7), 75% conversion of **1a** was observed but the yield of the desired product **3aa** was at the same level (6%, *E/Z* ratio 79:21). The formation of slight amount of product in both cases, confirms a crucial role of thiol in formation of the XAT reagent. At the same time, the formation of the product indicates an operation of alternative mechanism delivering  $CO_2^-$  intermediate. This could proceed by a mechanism reported by Yatham and coworkers,<sup>79</sup> postulating a formation of this radical anion directly from formate salt in the presence of dimsyl anion. Accordingly, they form EDA-complex which upon a purple light irradiation (390 nm) undergoes excitation to produce intermediate  $CO_2^-$ . Indeed, deepen analysis of UV spectra of **1a** +  $HCOOCs$  (e-SI, Fig. SI-5) allows to notice very slight absorption around 370 and 450 nm, however, this excitation is too weak to have any influence on the process and can be neglected.

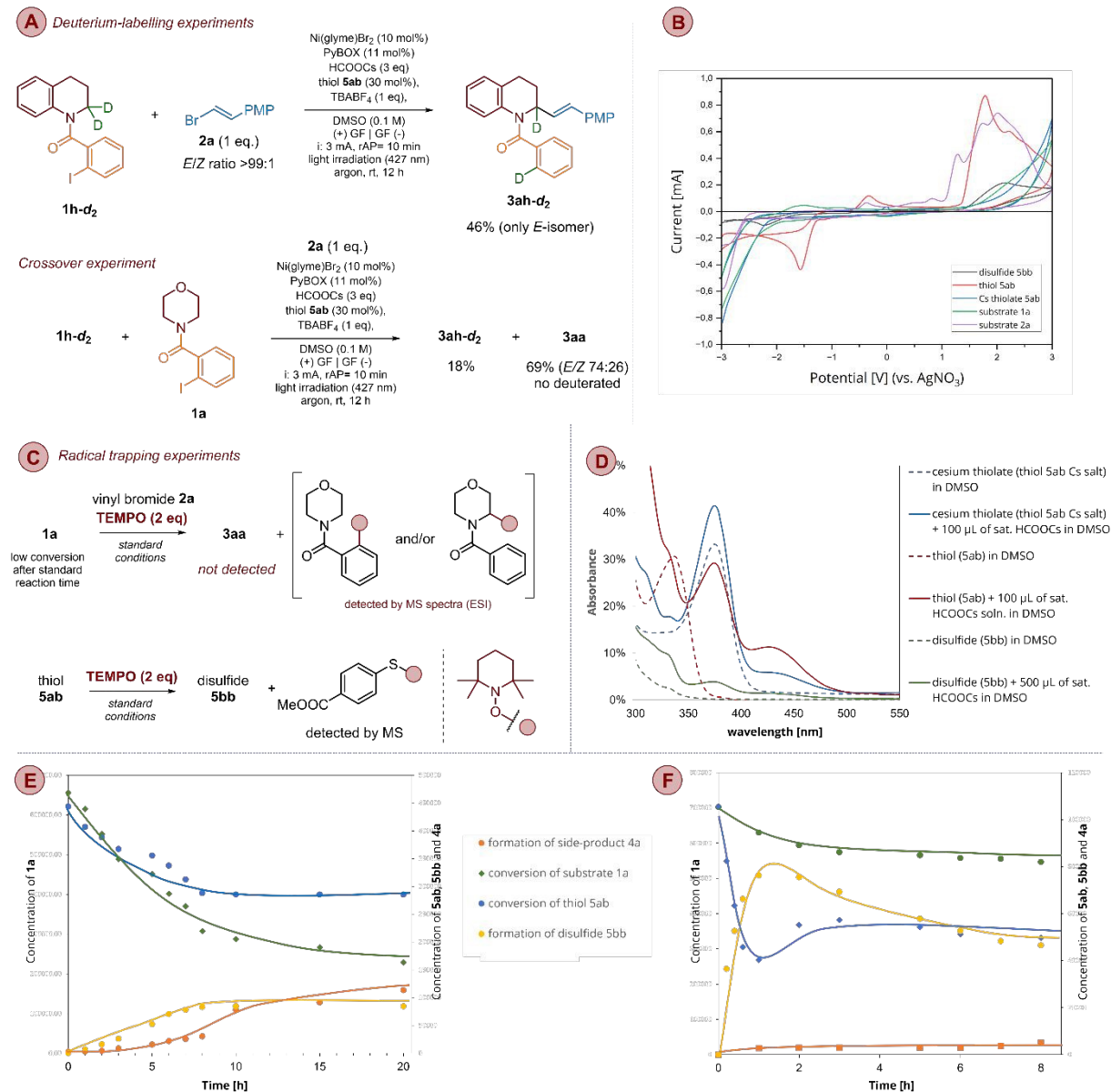
Finally, as indicated in Scheme 14 (ent. 10), the investigated process is slightly air sensitive; the experiments performed without inert gas yielded product **3aa** in ca. 70%, whereas, under argon atmosphere, the same product was obtained in 87% (ent. 1). Contrarily, the moisture is not allowed, as indicated by control experiments furnishing only traces of the desired product (ent. 11).

Considering that thiyl radicals may also function as hydrogen atom transfer (HAT) reagents, we conducted control experiments to exclude this possibility. Accordingly, compound **4a** was subjected to reaction with vinyl bromide **2a** under the standard reaction conditions (Scheme 14, ent. 12). After irradiation with blue light and passing an electric current for a standard 12 hours, no formation of the expected product **3aa** was observed. This result indicates that the neither  $ArS\cdot$  nor  $CO_2^-$  act as HAT reagents and are incapable of activating our starting material via cleavage of the  $C(sp^3)-H$  bond.

Deuterium-labelling and crossover experiments indicated that the reaction exclusively underwent intramolecular 1,5-HAT processes, additionally ruling out intermolecular hydrogen atom abstraction (Scheme 15a) and are in agreement with related studies previously reported.<sup>47, 55, 103</sup>

The addition of a radical trapping reagent, such as TEMPO, effectively inhibited the reaction, and only partial conversion of substrate **1a** was observed. Mass spectrometric analysis of the crude reaction mixture revealed the presence of products resulting from the interception of radical species,

specifically, aryl radicals and/or  $\alpha$ -aminoalkyl radicals (Scheme 15c & e-SI, Fig. SI-1a) and aryl thiyl radical (Scheme 15b & e-SI, Fig. SI-1b), by TEMPO. Notably, the expected product **3aa** was not detected in the crude reaction mixture (see e-SI, §9.1).

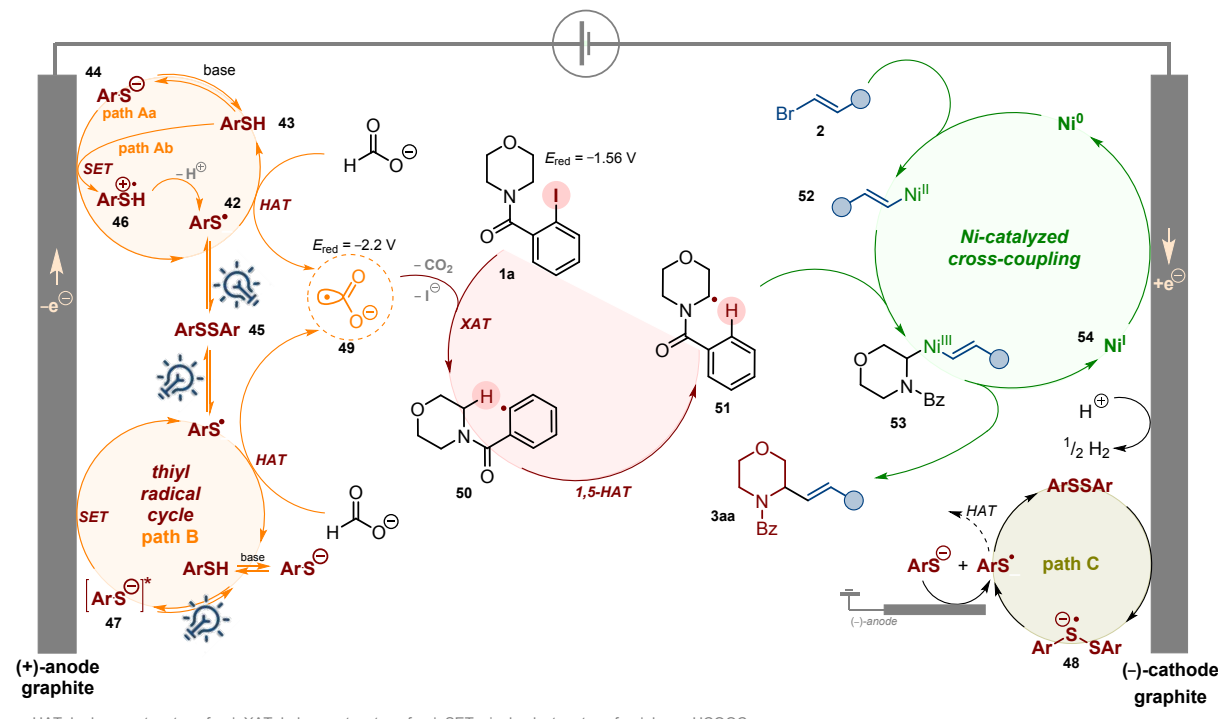


**Scheme 15.** Mechanistic studies: (A) deuterium-labelling and cross-over experiments; (B) cyclic voltamperograms of key reagents; (C) radical trapping experiments with TEMPO; (D) UV-Vis spectra of thiol **5ab**, its Cs salt and disulfide **5bb** with and without addition of HCOOCs in DMSO; (E) Kinetic studies of the model reaction without light; (F) Kinetic studies of model reaction (standard conditions).

The above disclosed observations, along with additional physicochemical measurements, including UV-Vis spectra (Scheme 15d, e-SI, §9.3) and CV measurements (Scheme 15b, e-SI, §9.4), allowed us to propose the plausible mechanism that is shown in Scheme 16. The key step is the formation of aryl thiyl radical **42**, a strong HAT reagent,<sup>104</sup> capable of a H-atom abstraction from formate salt to deliver highly reducing  $\text{CO}_2^{\cdot-}$  species **49** ( $E_{1/2}(\text{CO}_2/\text{CO}_2^{\cdot-}) = -2.2$  V).<sup>78, 80, 105, 106</sup> Radical anion **49** reduces substrate **1a** ( $E_{\text{red}} = -1.56$  V) via XAT process, furnishing aryl radical **50** capable of the subsequent 1,5-HAT process to afford nucleophilic  $\alpha$ -aminoalkyl radical **51**. Meanwhile, vinyl bromide



**2a** undergoes oxidative addition with the Ni(0) complex to form Ni(II)-complex **52**. Then, complex **52** intercepts radical **51** to provide Ni(III)-complex **53**. The final reductive elimination furnishes product **3aa** and Ni(I) intermediate **54**. The latter one is then reduced to Ni(0) to close the Ni-catalytic cycle. This final reduction is realized as a cathodic process, which is essential for the efficiency of the investigated reaction sequence. As already mentioned, without electric current, the product yield cannot exceed 10%, which is equal to the Ni catalyst loading.



**Scheme 16.** Proposed mechanism for  $\alpha$ -C(sp<sup>3</sup>)-H alkenylation of saturated heterocycles.

We have considered two alternative mechanisms to generate thiyl radical **42** presented in Scheme 16. The first mechanism assumes anodic oxidation of thiol **43** (via radical cation **46** following deprotonation, path Aa) or thiolate **44** (path Ab) to thiyl radical **42** which rapidly dimerizes to disulfide **45**. Photo-induced homolysis of the S-S bond in **45** delivers aryl thiyl radical **42** which dimerizes again or reacts with formate, delivering intermediate **49**. At the same time, the resulting disulfide **45** could take one electron from cathode, leading to disulfide radical anion **48** which decomposes to the thiyl radical **42** and thiolate **44** (path C). The thiolate anion can be converted again to the thiyl radical at the anode and the latter one dimerizes or acts as a HAT reagent.<sup>107, 108</sup>

On the other hand, it is the well-known fact that arene thiolate anions, formed by thiol deprotonation with a weak base, may absorb visible light and participate in a photoredox cycle.<sup>109</sup> Therefore, we considered an alternative mechanism, presented in Scheme 16 (path B), in which, an irradiation of **44** generates excited thiolate **47**, which undergoes a subsequent anodic SET process to deliver thiyl radical **42**.

To determine the mechanism of the generation of radical **42**, we measured UV-Vis absorption spectra to detect the light-absorbing species in the reaction mixture (Scheme 15c & e-SI, §9.3). Neither **1a** nor **2a** absorbed visible light in the operational range of 390–430 nm, which eliminated them as potent photoactive species (see e-SI, Fig. SI-5 and SI-6). An addition of HCOOCs to **1a** provided a slight bathochromic shift of the band, but still the observed absorption was out of the investigated range of wavelengths (see e-SI, Fig. SI-6). The UV-Vis studies also excluded the thiol **5ab** as a photoactive species because its absorbance was also out of the operating light window ( $\lambda_{\text{max}}$  337 nm) (Scheme 15c). As already mentioned, arene thiolate anions may absorb visible light and participate in a photoredox cycle because their HOMO energy is higher than that of the neutral thiol.<sup>109</sup> Indeed, UV spectra of deprotonated thiol **5ab**, obtained by its treatment with  $\text{Cs}_2\text{CO}_3$ , showed a bathochromic shift of absorption to ca. 375 nm, along with an increase of an absorption intensity (Scheme 15c). Although such absorbance onset overlaps with emission of employed light source at 395 nm, it does not rationalize why less energetic blue light is also suitable to execute C-H alkenylation efficiently. The answer came after measure an absorption spectrum of thiol **5ab** after an addition of HCOOCs as a base instead of  $\text{Cs}_2\text{CO}_3$ . The recorded spectra gave almost exact absorption curve with characteristic red-shifted band at 375 nm (Scheme 15c). However, there was additional weak band ca. 425 nm, which missed in case of cesium thiolate UV-Vis data. Finally, when cesium thiolate and HCOOCs were mixed together, the absorption curve was the same with the one for thiol/HCOOCs mixture, along with similar green emission as showed in Scheme 15d. The appearance of mentioned band at ca. 425 nm suggests that thiolate may interact also with formate anion(s) to give certain type of donor-acceptor complex that is photoactive species in the reaction. Noteworthy, the formate salt counterion has no influence on spectroscopic properties of UV spectra, and the same curve was obtained for thiol mixed with Li, Na, K, Cs,  $\text{NH}_4$  formates as well as tetra-*n*-butylammonium (TBA) formate (see e-SI, Fig. SI-12).

To confirm the formation of the excited species **47** and elucidate its role in the proposed mechanism, fluorescence quenching experiments were conducted using photoexcited anion **47**. The addition of varying amounts of the potent quencher, like substrate **1a**, to a mixture of thiol **5ab** and HCOOCs in DMSO did not result in a decrease in emission at either 428 nm (excitation at 375 nm) or 527 nm (excitation at 425 nm). Instead, increasing the concentration of **1a** led to an enhancement of emission intensity, suggesting that **1a** acts as a fluorescence sensitizer or energy donor, rather than as a quencher. While these findings do not rule out pathway B, they allow us to conclude that the excited anion **47** is not directly involved in the activation of starting materials **1a** and **2a** (see e-SI, §9.3.2).

As previously demonstrated, the C-H alkenylation of **1a** also proceeded when thiol **5ab** was replaced by disulfide **5bb**, affording product **3aa** in 51% yield (Scheme 14, entry 9). Given that disulfides can be readily prepared via oxidative coupling of thiols,<sup>110</sup> we hypothesized that similar oxidative coupling could occur under our reaction conditions. Specifically, disulfide **45** is expected to undergo photolysis of its weak S-S bond, generating the key arene thiyl radical **42**. Indeed, the MS and GC analysis of crude reaction mixtures from C-H alkenylation experiments conducted in the presence of thiol **5ab** revealed the presence of disulfide **5bb**, supporting our hypothesis. Furthermore, control experiments in which a DMSO solution of thiol **5ab** was electrolyzed in the presence of  $\text{TBABF}_4$  as



electrolyte confirmed the formation of **5bb** under reaction conditions, which was isolated in 73% yield. Volume Online  
DOI: 10.1039/D5SC08559D

(see e-SI, §8.4).

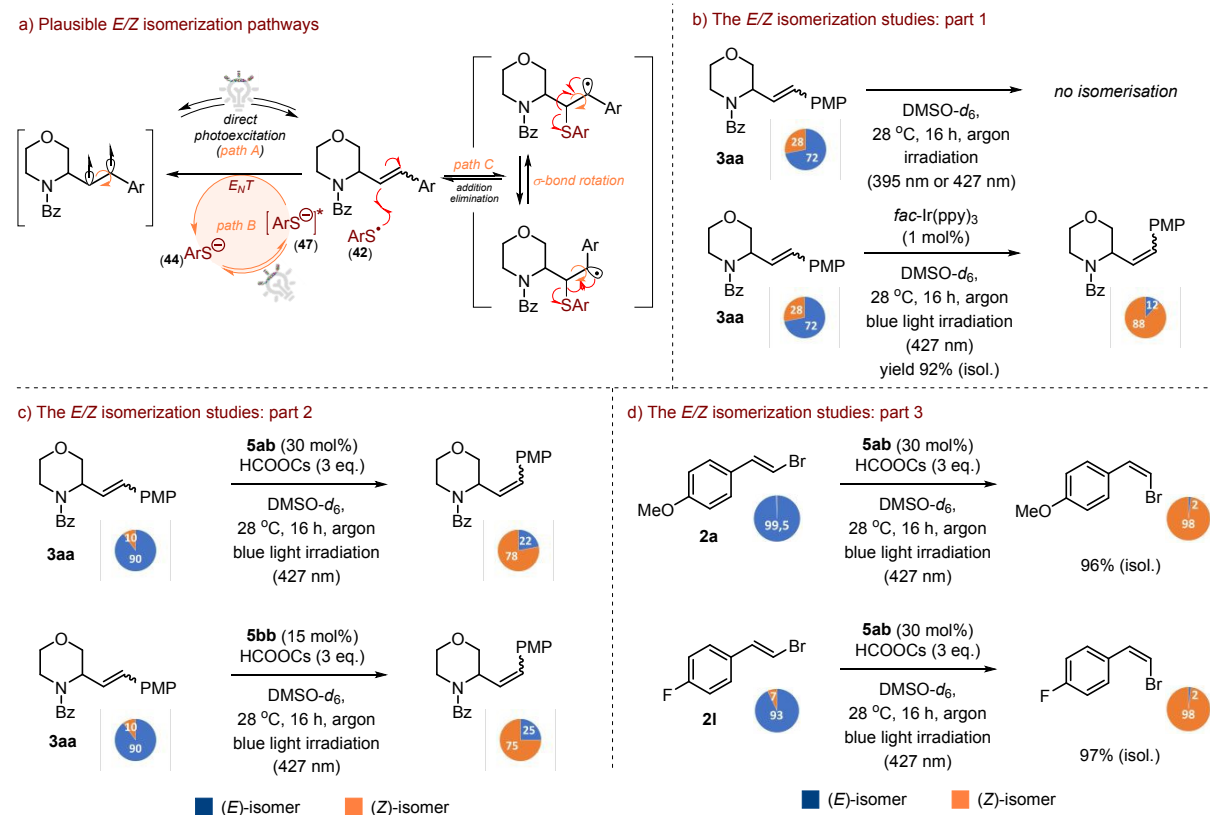
As shown in Scheme 14, entry 2, the reaction performed in the absence of light yielded only trace amounts of the desired product, suggesting that the generation of thiyl radical from disulfide via cathodic reduction (path C) either does not occur or proceeds at a rate where dimerization of the thiyl radical outpaces H-atom abstraction. Kinetic experiments appear to support the latter scenario. As shown in Scheme 15e, under dark conditions, substrate **1a** undergoes slow conversion, forming primarily coupling byproducts. Simultaneously, the concentration of thiol **5ab** decreases and stabilizes within approximately 6 hours, while the concentration of disulfide increases to a constant level during the same period. This suggests the establishment of an equilibrium between RSH and RSSR, resulting in insufficient levels of thiyl radical species to promote the designed reaction sequence. Notably, gas chromatography analysis showed only trace amounts (3%) of the desired product after 20 hours.

Upon irradiation of the reaction mixture, the kinetic profile changed significantly (Scheme 15f). In control experiments under blue light irradiation (without formate), the concentration of thiol **5ab** rapidly decreased during the first 60 minutes, then gradually increased to a stable level after approximately three hours. Concurrently, the concentration of disulfide **5bb** initially increased rapidly, then slightly decreased and stabilized after about three hours.

These observations support two possible hypotheses. The first posits that light irradiation shifts the thiol/disulfide equilibrium by promoting homolytic cleavage of the disulfide S-S bond, thereby generating thiyl radicals. While thiol dimerization continues, photolysis ensures a continuous supply of aryl thiyl radicals, facilitating the generation of  $\text{CO}_2^-$  and initiating the sequence of XAT, 1,5-HAT, and cross-coupling processes. Alternatively, the second hypothesis suggests that light activates an alternate pathway (such as path B), enabling rapid consumption of thiol, possibly through a rapid anodic oxidation of species **47** to radical **42**. Simultaneously, both paths A and C may operate too, converting excess of the reactive thiyl radicals into disulfide, which serves as a reservoir and maintains their effective concentration to initiate all intended transformations, thereby enabling the formation of  $\text{C}(\text{sp}^3)\text{-H}$  alkenylation products. Unfortunately, due to the complexity of the entire system, it is not possible to judge undoubtedly which pathway, A or B, dominates, therefore, it seems to be more appropriate to assume that both paths operate simultaneously along with cathodic transformations of disulfide (path C).

The last issue was an explanation of partial (*E/Z*)-isomerization of the C-H alkenylation for some products, although, in all examined cases pure (*E*)-isomers of vinyl bromides were used. Since our protocol does not use any of the common metal-based or organic photocatalysts, we considered two possible scenarios of observed double bond isomerization: 1) direct excitation of a double bond to diradical (path A), or 2) reactive species-promoted isomerization either via triplet energy transfer (path B)<sup>111, 112</sup> or an addition/elimination sequence (path C), as shown in Scheme 17a.<sup>104</sup> Moreover, the isomerization can either primary or secondary process depending on whether it deals to substrate, vinyl bromide, or product.

The initial control experiments, in which was directly irradiated either with purple (395 nm) or blue light (427 nm) excluded path A, since a blue (427 nm) or purple (395 nm) light irradiation of a solution of **3aa** (*E/Z* ratio 72:28) in DMSO did not reveal any change of the isomer ratio after 16 hours (Scheme 17b, eq. 1). Contrarily, in the control experiment, we have added *fac*-Ir(ppy)<sub>3</sub> to the solution of **3aa** in DMSO, and the resulting mixture was irradiated with blue light (427 nm). After 16 hours, an initial (*E/Z*)-isomers ratio of 72:28 changed leading predominately to contra-thermodynamic (*Z*)-isomer (*E/Z* ratio of 12:88) which was isolated in 92% yield (Scheme 17b, eq. 2).



**Scheme 17.** The *E/Z* isomerization studies.

Based on these two observations, additional control experiments were performed to determine the mechanism (path B or C) and identify active species involved in the isomerization process. Particularly, we focused on the arene thiyl radical as a potent isomerisation agent.<sup>104</sup> A blue light irradiation (427 nm) of a solution of (*E/Z*)-**3aa**, thiol **5ab** (30 mol%) and HCOOCs (3 equiv.) in DMSO resulted in a significant change of the (*E/Z*)-ratio from 90:10 to 22:78, after 16 h, with a dominance of the (*Z*)-isomer (Scheme 17c, eq 1). The same outcome was observed when thiol **5ab** was replaced by disulfide **5bb** (15 mol%). After standard time, 16 h, again the *E/Z*-isomers ratio changed from 90:10 to 25:75 (Scheme 17c, eq. 2). As can be seen from data collected in Scheme 4, the tendency for the partial formation of type-(*Z*)-**3** products was noticed only for mono-cyclic substrates **1**, which may suggest that *E*-to-*Z* isomerisation of a double bond, is easier for them due to their less steric hindrance and better accessibility to the double bond compared to fused systems. Furthermore, as disclosed in Scheme 8, the electronic nature of aryl group of vinyl bromides did not have significant influence on a (*E/Z*)-isomers ratio of product, and partial isomerisation was observed for both electron-rich, as well as electron-poor



system, without any strict trends. Thus, again confirms our statement about pivotal role of steric factors on final isomer ratio. As further experiments revealed, the starting (*E*)-vinyl bromides, e.g., **2a** and **2l**, can also be isomerized to (*Z*)-isomers in the presence of thiol and formate salt (Scheme 17d, eqs 1 & 2). The isomerization proceeded smoothly for electron-rich, like **2a**, as well as electron-deficient system, such as bromide **2l**.

It is important to emphasize that the isomerization our products, e.g., **3aa**, occurred only in the presence of HCOOCs. Otherwise, the (*E/Z*)-isomers ratio became almost unchanged (see e-SI, §8.2). The same dealt with the cases when the mixture of (*E/Z*)-**3aa** and HCOOCs without thiol or disulfide was exposed to blue light irradiation. This corresponds to our UV-Vis studies, which revealed that neither thiol **5ab** nor disulfide **5bb** absorbs the blue light with wavelength 427 nm. This again confirms the pivotal role of formate salt in the investigated process, not only as a precursor for XAT reagent ( $\text{CO}_2$  radical anion) but also as an essential activator for the generation of thiyl radical either from thiol or disulfide.

Analysis of the mass spectra of crude reaction mixtures from the isomerization experiments, as depicted in Schemes 17c and 17d, revealed the presence of very weak mass peaks potentially corresponding to aryl thiyl addition/hydrogen atom transfer (HAT) reaction products. The formation of these species appears to support our hypothesis regarding thiyl radical-induced double bond isomerization via an addition/elimination mechanism (path C), and is consistent with previous reports.<sup>104</sup>

To assess the plausibility of isomerization proceeding through the path B mechanism, fluorescence quenching experiments involving the excited thiolate species (**47**) were conducted. Emission spectra recorded upon excitation at 375 nm and 425 nm (see e-SI, Fig. SI-14) indicated that compound **3aa** could act as a potent quencher of the excited species **47**, although quenching was relatively weak, especially with excitation at the lower energy wavelength. This observation suggests that a significant interaction between species **47** and the product (or vinyl bromide) under the reaction conditions cannot be excluded, potentially facilitating double bond activation to a diradical species, for example via an energy transfer process as illustrated in Scheme 17a.

Nevertheless, the limited amount of currently available data, along with the inherent complexity of the reaction system, precludes unequivocal and definitive proof of isomerization via path B. Therefore, we are more inclined to attribute the observed partial isomerization of the products to path C as the most probable mechanism.

## Conclusions

In summary, we developed a general and mild photoelectrochemical method for  $\alpha$ - or  $\beta$ - $\text{C}(\text{sp}^3)\text{-H}$  alkenylation of various readily available monocyclic or benzofused amines using a series of vinyl



bromides. The established protocol accommodates a wide variety of amine scaffolds and vinyl bromides. Article Online DOI: 10.1039/D5SC08559D  
demonstrates tolerance for different functional groups, exhibits adequate *E/Z* selectivity, and shows slight sensitivity to oxygen. An Ni complex catalyses the installation of an alkenyl fragment, which results in limited compatibility with moisture. Mechanistic studies suggest that the transformation relies on the formation of aryl thiyl radical species, which react with formate to yield  $\text{CO}_2^-$ . This species acts as an XAT reagent capable of generating an aryl radical from the corresponding aryl iodide. Subsequently, the aryl radical abstracts an H-atom from the amine fragment through intramolecular 1,5-HAT, resulting in the formation of an  $\alpha$ -aminoalkyl radical, which is then intercepted by the Ni-alkenyl complex. Furthermore, we demonstrated that substituting the 2-iodobenzoyl HAT-directing group with its sulfonyl analogue facilitates a 1,6-HAT process, leading to  $\beta$ -alkenylated products. This method has shown significant applicability in the construction of complex heterocyclic scaffolds and in the late-stage functionalisation of bioactive molecules. Additionally, the resulting allyl- and homoallyl amine products can be readily transformed into various  $\alpha$ - and  $\beta$ -functionalised cyclic amines, thereby facilitating the synthesis of numerous nitrogen-containing heterocyclic natural products and pharmacoactive compounds. Consequently, the reported procedure is anticipated to have numerous applications in synthetic organic chemistry and medicinal chemistry, including drug discovery studies.

## Methods

In a glove box, oven dry an ElectraSyn vial (A) (10 mL) equipped with a magnetic stir bar was charged with vinyl bromide (0.6 mmol, 1.0 equiv), 2-halobenzamide (0.66 mmol, 1.1 equiv), HCOOCs (1.8 mmol, 3.0 equiv), methyl 4-mercaptopbenzoate **5ab** (0.12 mmol, 0.2 equiv) and *n*-Bu<sub>4</sub>NBF<sub>6</sub> (0.6 mmol, 1.0 equiv). The vial was closed with a PTFE cap equipped with anode (graphite) and cathode (graphite). In another oven dry 5 ml vial (B) was charged with Ni(glyme)Br<sub>2</sub> (0.06 mmol, 0.1 equiv) and PyBOX ligand **L8a** (0.066 mmol, 0.11 equiv). Magnetic stir bar was added and vial B was closed with septa cap. Both vials were taken out from a glove box and kept under argon. In as Vial A 4ml Under argon dry DMSO was added to both vials; 4 mL to the vial A and 2 mL to the vial B. The mixture in the vial B was kept stirred at 60°C for 10 min to prepare pre-nickel complex. After that time, solution of Ni-complex was transferred from the vial B to the vial A. which was added to vial A. Now, the vial A was installed on an ElectraSyn stand and electrolysis was started (Constant current 3 mA, time 12 h, alternating electrodes polarity change every 10 min) along with blue light irradiation by Kessil™ LED lamp (427 nm, 5 cm away, with cooling fan to keep the reaction temperature at 25 °C) for 12 h. After completion of the reaction, the reaction mixture was transferred to a separatory funnel, the electrodes were rinsed with ethyl acetate (5 mL) and water. The aqueous layer was extracted with ethyl acetate (3 × 20 mL). The combined organics were washed successively with brine (1 × 30 mL), then dried over MgSO<sub>4</sub> or Na<sub>2</sub>SO<sub>4</sub>. After removal of drying agent, solvents and volatiles were removed on a rotary evaporator. The crude product was purified via automated flash chromatography. The obtained product was kept for under high vacuum (10<sup>-3</sup> bar) at 70°C in the Kugelrohr apparatus for 10h to remove the traces of solvents. The progress of the reaction was followed by TLC by using UV (254 nm) detection and vanillin stain. *E/Z*-isomers ratio was assigned by <sup>1</sup>H NMR or GC analysis.



## Acknowledgements

View Article Online  
DOI: 10.1039/D5SC08559D

Authors are grateful to National Science Center of Poland for a financial support by research grant (OPUS 2021/43/B/ST4/019115)

## Declaration of no conflict

The Authors declare no conflict of interest.

## Electronic Supplementary Materials

Synthetic procedures, equipment setup, optimisation studies, characterisation of organic compounds, photochemical studies, copies of  $^1\text{H}$ ,  $^{13}\text{C}$ ,  $^{19}\text{F}$  NMR spectra. The Supporting Information is available free of charge.

## References:

1. A.-j. Deng and H.-l. Qin, *Phytochem.*, 2010, **71**, 816-822.
2. P. Huang, P. Cheng, M. Sun, X. Liu, Z. Qing, Y. Liu, Z. Yang, H. Liu, C. Li and J. Zeng, *Med. Plant Biol.*, 2024, **3**.
3. X. Luo, L. Pedro, V. Milic, S. Mulhovo, A. Duarte, N. Duarte and M.-J. U. Ferreira, *Planta Med.*, 2012, **78**, 148-153.
4. X. Luo, D. Pires, J. A. Aínsa, B. Gracia, N. Duarte, S. Mulhovo, E. Anes and M.-J. U. Ferreira, *J. Ethnopharm.*, 2013, **146**, 417-422.
5. Y. G. Xia, G. Y. Li, J. Liang, B. Y. Yang, S. W. Lü and H. X. Kuang, *Evid Based Complement Alternat Med*, 2014, **2014**, 684508.
6. S. G. Davies, A. M. Fletcher, I. T. T. Housby, P. M. Roberts, J. E. Thomson and D. Zimmer, *J. Nat. Prod.*, 2018, **81**, 2731-2742.
7. I. Jacquemond-Collet, F. Benoit-Vical, M. Valentin, A. Stanislas, E. Mallié, M. Fourasté and Isabelle, *Planta Med*, 2002, **68**, 68-69.
8. A. J. Aladesanmi, C. J. Kelley and J. D. Leary, *J. Nat. Prod.*, 1983, **46**, 127-131.
9. E. Tojo, M. A. Önür, A. J. Freyer and M. Shamma, *J. Nat. Prod.*, 1990, **53**, 634-637.
10. S. Dayot, D. Speisky, A. Couvelard, P. Bourgoin, V. Gratio, J. Cros, V. Rebours, A. Sauvanet, P. Bedossa, V. Paradis, P. Ruszniewski, A. Couvineau and T. Voisin, *Oncotarget*, 2018, **9**.
11. P. Malherbe, E. Borroni, E. Pinard, J. G. Wettstein and F. Knoflach, *Mol. Pharm.*, 2009, **76**, 618-631.
12. DrugBank.com: Iferanserin, <https://go.drugbank.com/drugs/DB11686>.
13. DrugBank.com: Encainide, <https://go.drugbank.com/drugs/DB01228>.
14. M. J. Antonaccio, A. W. Gomoll and J. E. Byrne, *Cardiovasc. Drugs Ther.*, 1989, **3**, 691-710.
15. R. L. Grange, E. A. Clizbe and P. A. Evans, *Synthesis*, 2016, **48**, 2911-2968.
16. A. K. Mailyan, J. A. Eickhoff, A. S. Minakova, Z. Gu, P. Lu and A. Zakarian, *Chem. Rev.*, 2016, **116**, 4441-4557.
17. S. L. Rössler, D. A. Petrone and E. M. Carreira, *Acc. Chem. Res.*, 2019, **52**, 2657-2672.
18. Q. Cheng, H.-F. Tu, C. Zheng, J.-P. Qu, G. Helmchen and S.-L. You, *Chem. Rev.*, 2019, **119**, 1855-1969.
19. O. Pàmies, J. Margalef, S. Cañellas, J. James, E. Judge, P. J. Guiry, C. Moberg, J.-E. Bäckvall, A. Pfaltz, M. A. Pericàs and M. Diéguet, *Chem. Rev.*, 2021, **121**, 4373-4505.
20. Y. Huang, R.-Z. Huang and Y. Zhao, *J. Am. Chem. Soc.*, 2016, **138**, 6571-6576.
21. B. M. Trost, C.-I. Hung and G. Mata, *Angew. Chem. Int. Ed.*, 2020, **59**, 4240-4261.
22. O. I. Afanasyev, E. Kuchuk, D. L. Usanov and D. Chusov, *Chem. Rev.*, 2019, **119**, 11857-11911.

23. R. A. Fernandes, P. Kattanguru, S. P. Gholap and D. A. Chaudhari, *Org. Biomol. Chem.*, 2017, **15**, 2672-2710. Article Online DOI: 10.1039/D5SC08559D

24. Y. Ichikawa, *Synlett*, 2007, **2007**, 2927-2936.

25. P.-A. Nocquet, S. Henrion, A. Macé, B. Carboni, J. M. Villalgordo and F. Carreaux, *Eur. J. Org. Chem.*, 2017, **2017**, 1295-1307.

26. R. Karl Dieter and R. R. Sharma, *Tetrahedron Lett.*, 1997, **38**, 5937-5940.

27. R. K. Dieter, C. M. Topping, K. R. Chandupatla and K. Lu, *J. Am. Chem. Soc.*, 2001, **123**, 5132-5133.

28. D. Antermite and J. A. Bull, *Synthesis*, 2019, **51**, 3171-3204.

29. E. N. Bahena, S. E. Griffin and L. L. Schafer, *J. Am. Chem. Soc.*, 2020, **142**, 20566-20571.

30. L. Li, Y.-C. Liu and H. Shi, *J. Am. Chem. Soc.*, 2021, **143**, 4154-4161.

31. A. L. Krasovskiy, S. Haley, K. Voigtritter and B. H. Lipshutz, *Org. Lett.*, 2014, **16**, 4066-4069.

32. E. Bisz, M. Koston and M. Szostak, *Green Chem.*, 2021, **23**, 7515-7521.

33. R. N. Shakhmaev, A. S. Sunagatullina and V. V. Zorin, *Russ. J. Org. Chem.*, 2014, **50**, 322-331.

34. M. Garbacz and S. Stecko, *Org. Biomol. Chem.*, 2021, **19**, 8578-8585.

35. M. Garbacz and S. Stecko, *Org. Biomol. Chem.*, 2023, **21**, 115-126.

36. A. Noble and D. W. C. MacMillan, *J. Am. Chem. Soc.*, 2014, **136**, 11602-11605.

37. Y.-T. Wang, Y.-L. Shih, Y.-K. Wu and I. Ryu, *Adv. Synth. Catal.*, 2022, **364**, 1039-1043.

38. Z. Qing, H. Cao, P. Cheng, W. Wang, J. Zeng and H. Xie, *Org. Chem. Front.*, 2018, **5**, 353-357.

39. M. Nechab, S. Mondal and M. P. Bertrand, *Chem. Eur. J.*, 2014, **20**, 16034-16059.

40. W. Guo, Q. Wang and J. Zhu, *Chem. Soc. Rev.*, 2021, **50**, 7359-7377.

41. L. Capaldo, D. Ravelli and M. Fagnoni, *Chem. Rev.*, 2022, **122**, 1875-1924.

42. L. Capaldo and D. Ravelli, *Eur. J. Org. Chem.*, 2017, **2017**, 2056-2071.

43. W. Li and C. Zhu, in *Remote C-H Bond Functionalizations*, 2021, DOI: 10.1002/9783527824137.ch11, pp. 315-341.

44. S. Sarkar, K. P. S. Cheung and V. Gevorgyan, *Chem. Sci.*, 2020, **11**, 12974-12993.

45. L. M. Stateman, K. M. Nakafuku and D. A. Nagib, *Synthesis*, 2018, **50**, 1569-1586.

46. S. Sarkar, S. Wagulde, X. Jia and V. Gevorgyan, *Chem.*, 2022, **8**, 3096-3108.

47. R. Guo, H. Xiao, S. Li, Y. Luo, J. Bai, M. Zhang, Y. Guo, X. Qi and G. Zhang, *Angew. Chem. Int. Ed.*, 2022, **61**, e202208232.

48. J. Wang, Q. Xie, G. Gao, H. Li, W. Lu, X. Cai, X. Chen and B. Huang, *Org. Chem. Front.*, 2023, **10**, 4394-4399.

49. M. G. Pizzio, E. G. Mata, P. Dauban and T. Saget, *Eur. J. Org. Chem.*, 2023, **26**, e202300616.

50. V. Srinivasu, K. Pal, S. Giri and D. Sureshkumar, *Org. Lett.*, 2024, **26**, 10328-10333.

51. Z. Lei, W. Zhang and J. Wu, *ACS Catalysis*, 2023, **13**, 16105-16113.

52. X. Lin, H. Huang, F. Yang, Y. Ren, Y. Gao and W. Su, *Org. Chem. Front.*, 2025, **12**, 829-837.

53. J. Zheng, H. Zhang, S. Kong, Y. Ma, Q. Du, B. Yi, G. Zhang and R. Guo, *ACS Catalysis*, 2024, **14**, 1725-1732.

54. H. Zhang, W. Gu, Q. Li, J. Zheng, J. Xiao, Y. Kang, W. Kandegama, X. Qi, G. Zhang and R. Guo, *ACS Catalysis*, 2025, **15**, 15425-15434.

55. J. Lu, K. Yuan, J. Zheng, H. Zhang, S. Chen, J. Ma, X. Liu, B. Tu, G. Zhang and R. Guo, *Angew. Chem. Int. Ed.*, 2024, **63**, e202409310.

56. M. Garbacz and S. Stecko, *Adv. Synth. Catal.*, 2020, **362**, 3213-3222.

57. S. K. Kariofillis, B. J. Shields, M. A. Tekle-Smith, M. J. Zacuto and A. G. Doyle, *J. Am. Chem. Soc.*, 2020, **142**, 7683-7689.

58. A. Q. Cusumano, B. C. Chaffin and A. G. Doyle, *J. Am. Chem. Soc.*, 2024, **146**, 15331-15344.

59. X.-C. He, K.-R. Li, J. Gao, J.-P. Guan, H.-B. Chen, H.-Y. Xiang, K. Chen and H. Yang, *Org. Lett.*, 2023, **25**, 4056-4060.

60. T. Constantin, F. Juliá, N. S. Sheikh and D. Leonori, *Chem. Sci.*, 2020, **11**, 12822-12828.

61. Z. Li, W. Yan, X. Zhou, C. Yang, L. Guo and W. Xia, *Org. Chem. Front.*, 2025, **12**, 4946-4955.

62. D. Kobus-Bartoszewicz, M. Zalewski, K. Melcer, M. Warda and S. Stecko, *Adv. Synth. Catal.*, 2025, **367**, e202401326.



63. S. Wang, C. Yang, S. Sun and J. Wang, *Chem. Commun.*, 2019, **55**, 14035-14038.

64. Y. Lai, A. Halder, J. Kim, T. J. Hicks and P. J. Milner, *Angew. Chem. Int. Ed.*, 2023, **62**, e202310246.

65. A. A. Folgueiras-Amador, A. E. Teuten, M. Salam-Perez, J. E. Pearce, G. Denuault, D. Pletcher, P. J. Parsons, D. C. Harrowven and R. C. D. Brown, *Angew. Chem. Int. Ed.*, 2022, **61**, e202203694.

66. K. Mondal, S. Mallik, S. Sardana and M. Baidya, *Org. Lett.*, 2023, **25**, 1689-1694.

67. Y. Kwon, J. Lee, Y. Noh, D. Kim, Y. Lee, C. Yu, J. C. Roldao, S. Feng, J. Gierschner, R. Wannemacher and M. S. Kwon, *Nature Commun.*, 2023, **14**, 92.

68. A. F. Chmiel, O. P. Williams, C. P. Chernowsky, C. S. Yeung and Z. K. Wickens, *J. Am. Chem. Soc.*, 2021, **143**, 10882-10889.

69. Z. Li, W. Yan, X. Zhou, C. Yang, L. Guo and W. Xia, *Org. Chem. Front.*, 2025, DOI: 10.1039/D5QO00479A.

70. L. W. Souza, N. D. Ricke, B. C. Chaffin, M. E. Fortunato, S. Jiang, C. Soylu, T. C. Caya, S. H. Lau, K. A. Wieser, A. G. Doyle and K. L. Tan, *J. Am. Chem. Soc.*, 2025, **147**, 18747-18759.

71. Kessil Lighting Ltd. Website. Kessil LED lamps Series PR160L specification for Kessil-PR160L-440nm ([https://kessil.com/products/science\\_PR160L.php](https://kessil.com/products/science_PR160L.php))

72. K. Grudzień, A. Zlobin, J. Zadworny, K. Rybicka-Jasińska and B. Sadowski, *Org. Chem. Front.*, 2024, **11**, 5232-5277.

73. M. Yan, Y. Kawamata and P. S. Baran, *Chem. Rev.*, 2017, **117**, 13230-13319.

74. S. R. Waldvogel, S. Lips, M. Selt, B. Riehl and C. J. Kampf, *Chem. Rev.*, 2018, **118**, 6706-6765.

75. X.-Q. Zhou, P.-B. Chen, Q. Xia, T.-K. Xiong, X.-J. Li, Y.-M. Pan, M.-X. He and Y. Liang, *Org. Chem. Front.*, 2023, **10**, 2039-2044.

76. N. Kurono, E. Honda, F. Komatsu, K. Orito and M. Tokuda, *Tetrahedron*, 2004, **60**, 1791-1801.

77. W. H. Koppenol and J. D. Rush, *J. Phys. Chem.*, 1987, **91**, 4429-4430.

78. Q. Shen, K. Cao, X. Wen and J. Li, *Adv. Synth. Catal.*, 2024, **366**, 4274-4293.

79. V. K. Simhadri, R. Sur and V. R. Yatham, *Eur. J. Org. Chem.*, 2024, **27**, e202400490.

80. C. M. Hendy, G. C. Smith, Z. Xu, T. Lian and N. T. Jui, *J. Am. Chem. Soc.*, 2021, **143**, 8987-8992.

81. M. C. Maust, C. M. Hendy, N. T. Jui and S. B. Blakey, *J. Am. Chem. Soc.*, 2022, **144**, 3776-3781.

82. L. Zeng, J. Wang, D. Wang, H. Yi and A. Lei, *Angew. Chem. Int. Ed.*, 2023, **62**, e202309620.

83. A. Bisoyi, A. Behera, A. R. Tripathy, V. K. Simhadri and V. R. Yatham, *J. Org. Chem.*, 2024, **89**, 17818-17823.

84. Z.-Y. Ma, L.-N. Guo, Y. You, F. Yang, M. Hu and X.-H. Duan, *Org. Lett.*, 2019, **21**, 5500-5504.

85. A. L. G. Kanegusuku, T. Castanheiro, S. K. Ayer and J. L. Roizen, *Org. Lett.*, 2019, **21**, 6089-6095.

86. M. A. Short, J. M. Blackburn and J. L. Roizen, *Synlett*, 2020, **31**, 102-116.

87. M. A. Short, M. F. Shehata, M. A. Sanders and J. L. Roizen, *Chem. Sci.*, 2020, **11**, 217-223.

88. P. L. Gkizis, I. Triandafillidi and C. G. Kokotos, *Chem*, 2023, **9**, 3401-3414.

89. J. K. Mitchell, W. A. Hussain, A. H. Bansode, R. M. O'Connor, D. E. Wise, M. H. Choe and M. Parasram, *Org. Lett.*, 2023, **25**, 6517-6521.

90. D. E. Wise, E. S. Gogarniou, A. D. Duke, J. M. Paolillo, T. L. Vacala, W. A. Hussain and M. Parasram, *J. Am. Chem. Soc.*, 2022, **144**, 15437-15442.

91. A. Ruffoni, C. Hampton, M. Simonetti and D. Leonori, *Nature*, 2022, **610**, 81-86.

92. K. Sun, Q.-Y. Lv, Y.-W. Lin, B. Yu and W.-M. He, *Org. Chem. Front.*, 2021, **8**, 445-465.

93. C. Pratley, S. Fenner and J. A. Murphy, *Chem. Rev.*, 2022, **122**, 8181-8260.

94. H. Zhang, C. Huang, X.-A. Yuan and S. Yu, *J. Am. Chem. Soc.*, 2022, **144**, 10958-10967.

95. M. Faizan, R. Kumar, A. Mazumder, Salahuddin, N. Kukreti, A. Kumar and M. V. N. L. Chaitanya, *Chem. Biol. Drug Discov.*, 2024, **103**, e14537.

96. R. R. Kumar, B. Sahu, S. Pathania, P. K. Singh, M. J. Akhtar and B. Kumar, *ChemMedChem*, 2021, **16**, 1878-1901.

97. A. F. Brito, L. K. S. Moreira, R. Menegatti and E. A. Costa, *Fund. Clin. Pharm.*, 2019, **33**, 13-24.



98. S. Singh, R. Kumar, S. Tripathi, Salahuddin, A. Mazumder and N. Singh, *Chem. Biol. Drug Discov.*, 2025, **105**, e70077. [View Article Online](#)  
DOI: 10.1039/D5SC08559D

99. R. B. Clark and D. Elbaum, *Tetrahedron*, 2007, **63**, 3057-3065.

100. Patent WO2003082877A1, 2003.

101. Patent WO2005026177A1, 2005.

102. US20050203296A1, 2005.

103. B. Ma, M. Ma, T. Zhang, D. Chen and J. Yang, *J. Org. Chem.*, 2025, **90**, 13643-13656.

104. F. Dénès, M. Pichowicz, G. Povie and P. Renaud, *Chem. Rev.*, 2014, **114**, 2587-2693.

105. W. Xiao, J. Zhang and J. Wu, *ACS Catalysis*, 2023, **13**, 15991-16011.

106. Y. Dang, J. Han, A. F. Chmiel, S. N. Alektiar, M. Mikhael, I. A. Guzei, C. S. Yeung and Z. K. Wickens, *J. Am. Chem. Soc.*, 2024, **146**, 35035-35042.

107. Y. Yuan, J.-C. Qi, D.-X. Wang, Z. Chen, H. Wan, J.-Y. Zhu, H. Yi, A. D. Chowdhury and A. Lei, *CCS Chemistry*, 2022, **4**, 2674-2685.

108. Y. Yuan, Y. Chen, S. Tang, Z. Huang and A. Lei, *Science Advances*, 2018, **4**, eaat5312.

109. C. Liu, K. Li and R. Shang, *ACS Catalysis*, 2022, **12**, 4103-4109.

110. G. Laudadio, N. J. W. Straathof, M. D. Lanting, B. Knoops, V. Hessel and T. Noël, *Green Chem.*, 2017, **19**, 4061-4066.

111. T. Neveselý, M. Wienhold, J. J. Molloy and R. Gilmour, *Chem. Rev.*, 2022, **122**, 2650-2694.

112. F. Strieth-Kalthoff and F. Glorius, *Chem*, 2020, **6**, 1888-1903.



Warsaw, Nov. 4<sup>th</sup>, 2025

To:

Editorial Office of Chemical Science

Dear Sirs,

**DATA AVAILABILITY**

The data supporting this article have been included as part of the Supplementary Information: this includes all experimental setup and details, materials used, optimization process of remote C-H alkenylation of amines, mechanistic studies, synthetic procedures, as well as the <sup>1</sup>H, <sup>13</sup>C, and <sup>19</sup>F NMR characterization data of the products.

Sincerely,

Siddharth Dave and Sebastian Stecko

Chemical Science Accepted Manuscript

